DETECTION OF CHARCOAL PRODUCTION SITES IN SOMALIA WITH VERY HIGH RESOLUTION AND SENTINEL-2 IMAGERY

TEOPISTA NAKALEMA
February, 2019

SUPERVISORS:
Dr. Ir. A Vrieling
Dr. Ir. T.A Groen

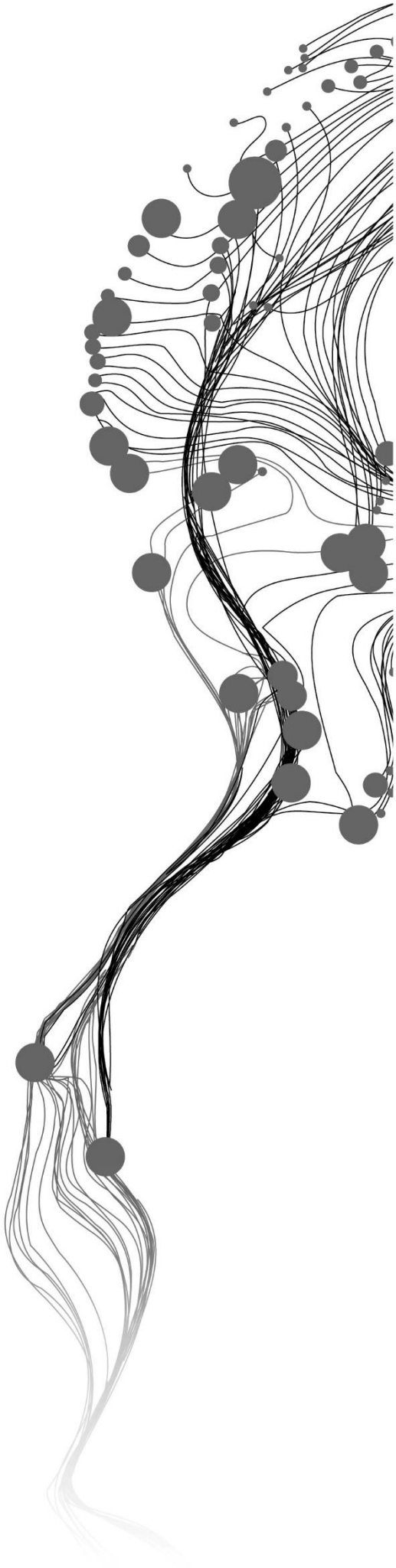

DETECTION OF CHARCOAL PRODUCTION SITES IN SOMALIA WITH VERY HIGH RESOLUTION AND SENTINEL-2 IMAGERY

TEOPISTA NAKALEMA
Enschede, The Netherlands, February, 2019

Thesis submitted to the Faculty of Geo-Information Science and Earth Observation of the University of Twente in partial fulfilment of the requirements for the degree of Master of Science in Geo-information Science and Earth Observation.
Specialization: Natural Resource Management

SUPERVISORS:
Dr. Ir. A Vrieling
Dr. Ir. T.A Groen

THESIS ASSESSMENT BOARD:
Dr. Y.A. Hussin (Chair)
Dr. F. Fava, International Livestock Research Institute, Nairobi, Kenya (External Examiner)

ABSTRACT

Despite a UN ban on the export of charcoal, charcoal production is still going on in Somalia leading to the degradation of the woody resources. Very High Resolution (VHR) images such as WorldView have been used to detect charcoal production sites to estimate the environmental degradation due to charcoal production. Because of their sub-meter spatial resolution, VHR images enable detection of charcoal sites. However, due to their high cost and limited area coverage, it is not feasible to use VHR images to map charcoal sites on a large scale and at a high temporal frequency. Therefore, this study explores the possibility of using freely available imagery from Sentinel-2 (10m) to detect and monitor charcoal sites in Somalia. As reference data, charcoal production sites were detected from multi-temporal VHR images in a 10x10km area near Kismayo in the Lower Juba region, Southern Somalia using a semi-automated workflow. A total of 1,740 sites were detected, out of which 439 were 'new' sites that were not detected on the earlier image (21 August 2016) but later in the study period until 12 August 2018. The average diameter of these sites was 8m. The new sites were then used to assess if the spatial and temporal variability in the surface reflectance derived from Sentinel-2 provides a clear signal that may allow for accurate detection of the charcoal sites. With the assumption that if a charcoal site appears, there will be a significant change in the spectral difference between the charcoal pixel and its surrounding, an approach to assess the reflectance of each pixel and the surrounding pixels over time was developed. The surrounding was defined as the outer pixels of a 5x5 pixel window around the site. The results show that for most of the charcoal sites tested, there was a significant increase in difference (i.e. surrounding minus charcoal pixel) during the appearance period of the site. This increase was most apparent in the NIR band of Sentinel-2 but not for all sites. To map charcoal sites for the full image and time series, a change in difference was computed at each point in time considering different temporal windows to reduce the noise due to clouds. The 180 days moving median performed better in terms of providing high maximum values for charcoal sites thus a threshold was determined to separate charcoal pixels from non-charcoal pixels. An optimal threshold of 400 (corresponding to 0.04 in reflectance) was set to ensure that none of the sample non-charcoal pixels were mapped as charcoal. Nonetheless, applying this threshold resulted in detecting merely 19% of the sample charcoal pixels and a number of non-charcoal pixels detected as charcoal. To further avoid the detection of non-charcoal pixels as charcoal, based on the sample pixels an additional criterion of a median reflectance of 0.18-0.25 of NIR reflectance for the 180 days after the maximum change-in-difference index was set. Therefore, two conditions based on the optimal threshold and NIR reflectance of the charcoal signal were applied to the entire Sentinel-2 time series to detect charcoal sites. A total of 671 pixels were detected as charcoal of which only 120 were actual charcoal sites as detected with VHR. This study demonstrates the potential of using Sentinel-2 time series in detecting charcoal sites whose sizes are below the spatial resolution of the sensor, but due to challenges such as clouds accurate detection is hindered. Further studies could benefit from incorporating a larger number of spectral bands and possibly spatio-temporal indices. For example by means of machine learning approaches, to automatically extract additional relevant information for charcoal detection from the Sentinel-2 time series for improving the accuracy of charcoal detection and monitoring on a large scale in Somalia.

Keywords: Charcoal production sites, VHR, Sentinel-2 time series, Somalia

ACKNOWLEDGEMENTS

First, my sincere gratitude goes to the Dutch government for the scholarship opportunity to study at the University of Twente, ITC. It has not only enabled me to grow professionally but also socially through interacting with students and people from all over the World. Great thanks go to my first supervisor Dr. Anton Vrieling for the technical support, guidance and fast feedbacks that put me on track throughout the entire period of my thesis. Also to my second supervisor Dr. Thomas Groen for the useful suggestions and comments. I thank the management of Somalia Water and Land Information Management (SWALIM), Nairobi Kenya for the internship opportunity to obtain VHR images from the DigitalGlobe Enhanced View Web Hosting (EVWH) archive. Special thanks go to Bolognesi Michele and Leonardi Ugo for the technical support and always making sure that everything was going fine during my short stay at SWALIM. I thank the staff of ITC especially in the Natural Resources Department for the knowledge that helped me in the implementation of my research. My fellow students and friends such as Mohammed Issamaldin Alshiekh, Yan Cheng, Paulina Peter Lokongo, Emmanuel Ocen, Virginiah Kamau and Clement Obeng-Manu for all the support and making my stay at ITC an enjoyable and memorable experience. I wish you all the best in your lives after ITC. I cannot forget to thank my colleagues; Edward Senyonjo, John Diisi, Antonia Ortmann, Yelena Finegold, Erik Lindquist, Remi Dannunzio, Rebecca Tavani at National Forestry Authority (NFA), Uganda and Food and Agriculture Organization (FAO) of the United Nations for the technical support and the confidence you have in me. To My family for the continuous encouragements and emotional support. I dedicate this work to my late mother Proscovia Nalunga who always believed in me and gave me the courage to believe in myself, may her soul rest in eternal peace

All in all, I thank the Almighty God for enabling me to successfully complete my research and the entire study at ITC.

TABLE OF CONTENTS

LIST OF FIGURES

LIST OF TABLES

LIST OF APPENDICES

1. INTRODUCTION

1.1. Background

Wood charcoal is a source of energy widely used in sub-Saharan Africa for cooking, heating, and generation of electricity (FAO, 2017). Charcoal is mostly used and preferred by urban dwellers because it is affordable, clean (produces less smoke), and has a higher energy density per unit weight (Iiyama et al, 2014). Use of other sources of energy such as solar, hydro-electric power and gas is low due to the fact that charcoal is relatively cheap making it affordable for most people. In the 1980s, firewood was the primary source of energy in African homes, but as urbanization and population grew, this shifted to charcoal leading to an increase in its production (Girard, 2002). In Africa, charcoal production is estimated to have increased from 29 million tonnes in 2012 to 32 million tonnes in 2016 accounting for 64% of the global production (FAO, 2016). Charcoal production is a source of income employing over 40 million people, thus helping in reducing unemployment in African countries (FAO, 2017). However, its increase together with lack of regulations and proper forest management presents a threat to the environment as it contributes to forest degradation and deforestation and their associated impacts such as floods, drought, soil erosion to mention a few (Girard, 2002). In addition, charcoal production contributes to global warming and climate change due to the emission of greenhouse gases such as carbon dioxide and methane into the atmosphere during the burning/heating of wood to produce charcoal in low oxygen conditions. Chidumayo and Gumbo (2013) estimated that in 2009 alone about 72.5 million tonnes of GHG were emitted from Africa due to charcoal production. They estimated that this corresponded to an equivalent of about 2,976,000 hectares of forest cleared for charcoal production in Africa accounting for 80% of charcoal-based deforestation on a global level. These estimates are alarming and if business continues as usual, charcoal production will help to rapidly deplete forest resources resulting in negative associated impacts.

Somalia is one of the African countries where charcoal production is a major concern leading to the depletion of the country's woody resources (FAO SWALIM, 2018). For over 30 years now the country has been under civil war, which resulted in increased exploitation of the natural resources by militia groups such as Al-Shabaab mostly in the central and southern parts of the country which are under their control. Charcoal trade is the main source of finance for Al-Shabaab, generating a revenue of over 15 USD per year to fuel war activities (UN, 2016). In order to control the import and export of charcoal in the country, many rules and regulations have been put in place. For example, in 2012, the UN Security Council (2012) banned the charcoal trade in Somalia for purposes of cutting off the main source of funding for Al-Shabaab, which would help bring back peace and stability in the country as well as reduce environmental degradation. However, the ban has been violated and the trade is still going on, despite that the UN Security Council has continued to reaffirm the ban in subsequent resolutions (UN Security Council, 2013, 2014, 2015, 2016, 2017). About 80% of the charcoal produced in Somalia is exported to the Gulf states while 20% is consumed domestically. About 250,000 tonnes of charcoal are estimated to be exported out of Somalia to the Gulf countries such as Saudi Arabia and Yemen every year translating into 4.4 million trees cut to turn into charcoal a year (Brown, 2013). The country is currently experiencing environmental related problems such as flooding and drought attributed in part to the massive forest degradation and deforestation since the country loses about 72,900 hectares of forest a year (Brown, 2013). Due to the fact that the trade is illegal and some areas are inaccessible like those under Al Shabaab's control, most of the charcoal produced is not recorded, thus underestimating the degradation due to

charcoal production in the country. In Somalia, charcoal is produced using the traditional earth kilns which are clearly visible on the ground (Robinson, 1988). Therefore, mapping these kilns would provide more reliable information by estimating tree loss as described by Bolognesi et al. (2015). In an ideal situation, ground observations of the kilns can be taken, but due to the insecurity issues in the country particularly in the southern parts, this is not possible. In addition, field visits are resource demanding where a lot of time and money would be required to map the kilns on a large scale. Therefore, remote sensing can assist to detect and map used charcoal kilns in Somalia, which can subsequently be used to estimate the associated degradation and deforestation in the country.

Charcoal sites are referred to as charcoal scars left on the ground after burning wood to convert it into charcoal which can be detected on remote sensing or satellite images due to their black or dark colour and circular or round shape (Rembold et al., 2013). On satellite images, the reflection of a charcoal site is similar to any burned area and because of the unique spectral signature, it is easy to discriminate burned areas from other surface features in the visible (VIS), near-infrared (NIR) and shortwave-infrared (SWIR) channels of multi-spectral sensors (Roy et al., 2002). Since the 1990s, many studies have used satellite images to map burned areas both at regional and global scales (Eva & Lambin, 1998; Roy et al, 2008; Roy et al, 2014; Humber et al, 2018). The Moderate Resolution Imaging Spectroradiometer (MODIS) is part of NASA's Earth Observing System onboard of the Terra and Aqua polar orbiting satellites whose data are being used to generate global burned areas products on a regular basis (Roy et al., 2014). Burned area indices such as the Burned Area Index (BAI) and Normalized Burned Ratio (NBR) based on the VIS, NIR, and SWIR spectral bands have been proposed and widely used for burned area mapping (Key & Benson, 2006). A number of studies have also explored the potential of using Sentinel-2 that was launched in 2015 to map burned areas (Huang et al., 2016; Colson et al., 2018; Roteta et al., 2019)

Despite the many studies on burned area mapping, few have looked at small scale mapping such as charcoal site detection. A study to operationalize the measurement of forest degradation for REDD+ project used pan-sharpened QuickBird images (0.6m) to identify charcoal production kilns in two sites with a history of charcoal production in the dry Miombo woodland, Tanzania (Dons et al., 2015). They reported a higher spectral separation of the burned areas from the surrounding with the NIR spectrum as compared to the visible range bands (blue, green and red). Because of the dark colour and circular shape of charcoal sites, Rembold et al. (2013) visually identified and counted charcoal production sites on WorldView-1 and QuickBird images to quantify forest degradation or tree loss in the Lower Juba region, southern Somalia. In the same region along the Juba river, Bolognesi et al. (2015) used a semi-automated approach to carry out a rapid mapping of illegal charcoal production sites using WorldView-1 imagery (0.5m). They detected a total of 18,042 charcoal sites in 2013 estimating a tree loss of 2.7% for an area of 4700 km^2 between 2011 and 2013. Because of the semi-automated approach, their research provides a basis for a need to scale up and map charcoal sites on a national level which can be used to quantify the degradation caused by charcoal production activity in Somalia. In order to achieve this, reliable remote sensing images are necessary. Very High Resolution (VHR) such as WorldView have the advantage of the sub-meter spatial resolution that enables easy detection of charcoal sites, but they are costly and have a limited area coverage. Therefore, there is a need to explore the freely available but high-resolution satellite images in mapping and monitoring of charcoal sites in Somalia.

The main aim of the study is to assess the possibility of using freely available medium resolution (10m) Sentinel-2 images in detecting and mapping charcoal production sites in Somalia. However, given the average size of three-meter radius of the charcoal sites as reported by (Bolognesi & Leonardi, 2018), the spatial resolution of Sentinel-2 may be too coarse to effectively detect the sites. This is due to the mixture of the charcoal signal with the surrounding land cover in a single pixel. In this case, ways of extracting and analysing the reflectance values of Sentinel-2 image are very important. For example, Spectral Mixture

Analysis (SMA) is a technique for estimating the proportion of each pixel that is covered by a series of known cover types and classify the pixel with the dominant land cover (Smith et al., 1994). This method has been successfully employed in a number of studies for land cover classification using remote sensing images (Adams et al., 1995; Fernández-Manso 2015; Tane et al., 2018; Fernández-Manso et al., 2009). However, in order to implement the SMA technique, the image to be classified should contain pure pixels of known endmembers that can be used to unmix the mixed pixels. For this study, pure pixels of charcoal sites may not be found in the Sentinel-2 images due to their relatively small size. Therefore a new approach is developed to analyse a charcoal pixel with its surrounding environment over time. To achieve this, the study first used VHR imagery from the DigitalGlobe archives to detect charcoal sites and to assess the timing of their appearance. The main focus of the study was then to detect new charcoal sites that appeared during the study period by assessing if the spatial and temporal variability in surface reflectance derived from Sentinel-2 can provide a clear signal that may allow accurate detection of these sites. The hypothesis in this assessment is that a significant change in the spectral reflectance occurs after a site is exposed and that this change persists for some time. If this approach would prove successful, it may enable mapping and monitoring of charcoal sites at a national level and at a higher temporal frequency, thus providing up-to-date information about dynamics of the charcoal production activity in Somalia for proper decision making

1.2. Reserch objective

To assess the temporal dynamics of charcoal production sites in southern Somalia with VHR imagery and test if spatio-temporal changes in surface reflectance from Sentinel-2 can provide a solid basis to accurately detect these sites.

Specific objectives

- To develop a semi-automated workflow to accurately detect charcoal production sites using VHR images;
- To precisely identify for each charcoal production site when it first appeared, until when it was visible, and if there is evidence for multiple use of the same site, based on VHR images;
- To assess if spatial and temporal variability in surface reflectance derived from Sentinel-2 provides a clear signal that may allow for accurately detecting the charcoal production sites;
- To map the location and timing of charcoal production sites using Sentinel-2 time series, and assess the accuracy of this mapping in relation to the VHR assessment.

2. STUDY AREA AND DATA

2.1. Study area

The study was conducted in the Lower Juba region of southern Somalia. The country has two rain seasons (Gu and Deyr). The main rain season (Gu) occurs between March to July and the second season (Deyr) between August to November but it varies across the country (Muchiri, 2007). The region and specifically near Kismayo receives an annual average rainfall of 366mm and has a temperature of 26.9 Degrees Celsius (Figure 1). The longest and driest season is between January to March and it is noted that the charcoal production activity mostly takes place during this period (Bolognesi & Leonardi, 2018). The vegetation in the region is mainly Acacia trees, coarse grasses and stunted thorn which are rapidly being depleted due to charcoal production (UN Security Council, 2011).

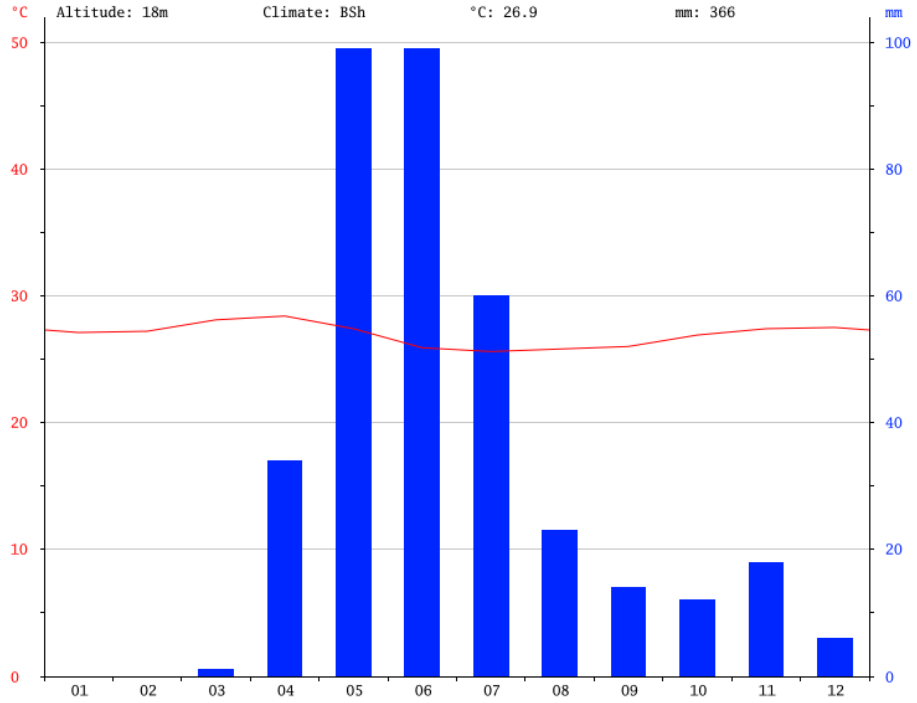

Figure 1: Temporal rainfall and temperature distribution at Kismayo, Lower Juba region (source: Climate-Data, 2017)

The study area was selected based on a research carried out by Bolognesi and Leonardi (2018), who assessed charcoal production sites and their dynamics from 2011 to 2017 in southern Somalia over an area of about 37,000 km2 using VHR images. They reported two areas near Kismayo and Buur Gaabo as having the highest densities of charcoal sites in 2017 as shown in Figure 2a. Due to the limited VHR images near Buur Gaabo, a square of 10x10km with centre coordinates (X=875252 and Y= 9992053) near Kismayo was selected for this study.

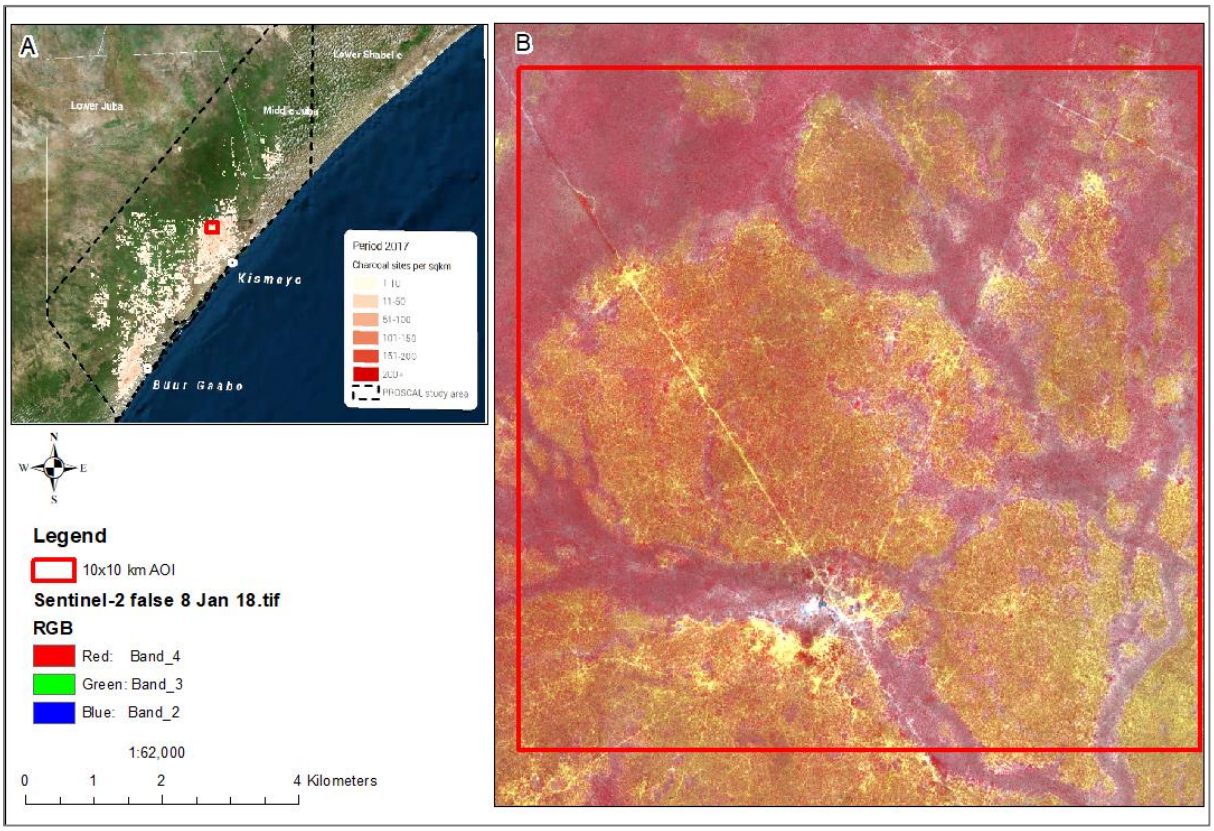

Figure 2: Study area: a) area of interest in a red polygon selected in areas of high charcoal densities and b) zoomed in area of interest with a false colour Sentinel-2 image shown in the background showing the general land cover of the area which is mainly shrub lands and bare soil with scattered trees.

2.2. Data

Two types of satellite data were used; Very High Resolution (VHR) from DigitalGlobe and Sentinel-2 imagery. Due to their sub-meter spatial resolution, VHR images allow to visually discern charcoal sites, which on average have a 3-meter radius (Bolognesi & Leonardi, 2018). VHR images were used to detect charcoal sites and assess the timing of their appearance with the purpose of identifying new sites that appeared during the study period. This information was later used to test if Sentinel-2 can also be used to detect the same sites. A study period from August 2016 to August 2018 was considered for the VHR images whereas for Sentinel-2 from January 2016 to December 2018. The selection of the study period was based on the availability of Sentinel-2 images since 2A was launched in 2015. A longer period was considered for Sentinel-2 to capture a clear pattern in the charcoal sites that appeared early or late in the study period of VHR.

2.2.1. VHR imagery

For this study, images of WorldView-1, WorldView-2, WorldView-3, and GeoEye-1 were obtained at the Somalia Water and Land Information Management (SWALIM) office of the Food and Agricultural Organization (FAO), Nairobi, Kenya from the DigitalGlobe Enhanced View Web Hosting (EVWH) archive. Eleven images of ten different dates were available and used, which either fully or partially covered the area of interest.

Table 1: VHR images used in the study

No.	Sensor name	Image date	Tiles used	FeatureId
1	WV02	8/21/2016	R2C1, R3C1, R3C2	f8d5dd0e0bf335dc200e1dc92b444716
2	WV02	10/25/2016	R8C1, R9C1	8f03ace4ec74db5258b9277f142dfbee
3	WV03_VNIR	1/16/2017	R11C1, R12C1	3295cfbc09027ea19f9bfe5c3acfc10e
4	WV03_VNIR	3/13/2017	R2C1,R3C1	9227524b83c23b84884c9a2f6921971b
5.1	WV03_VNIR	4/1/2017	R1C3, R2C2, R2C3, R3C3	449467b0aeb7045f76e85f72dd54b696
5.2	WV03_VNIR	4/1/2017	R2C1, R3C1	132a0026bbd54d41bfcc221ea3ebb810
6	WV02	4/19/2017	R2C1, R2C2	dca7b892a67260952114e15c216a00b1
7	WV02	4/27/2017	R1C1, R1C2, R2C1, R2C2, R3C1	223b90d4471d41ba46f3e662b2b39932
8	GE01	5/8/2017	R1C1, R2C1	afcdbea97d0cb6cb6a15e5e943770edb
9	WV02	6/4/2017	R1C2, R2C2	ca8973b4f93dc5898e8aa6e6ca789bb9
10	GE01	1/11/2018	R1C1, R2C1	69dba04f494bfebf26ad434c206bd99c
11	WV02	4/12/2018	R1C1, R1C2, R1C3, R2C2, R2C3	fd79247f2cea77a8e7fffdcc7334741c

The images were obtained from EVWH archive as pan-sharpened natural colour with blue, green and red spectral bands in WGS_1984_UTM_Zone_38S coordinate system and 0.5m spatial resolution. All images between August 2016 and August 2018 with 90% or less cloud cover were considered. This study period was chosen to be able to detect sites that appear during the two dry seasons of 2016-2017 and 2017-2018.

2.2.2. Sentinel-2

Sentinel-2 is an Earth observation satellite mission that provides 10-60m resolution images at frequent intervals and for free to support services such as land monitoring, emergency management, security and climate change (ESA, 2015). The mission has two twin satellites, i.e. Sentinel 2A and 2B, which were launched on 23 June 2015 and 7 March 2017 respectively. Together they provide a five-day revisit time at the equator. The multi-spectral instrument (MSI) of the satellites provide 13 bands; four bands at 10m, six bands at 20m, and three bands at 60m spatial resolution. For this study, six bands were used, that is band 2 (blue), band 3 (green), band 4 (red), band 8 (NIR), band 11 (SWIR1) and band 12 (SWIR2) (Table 2). The four 10m bands were chosen because they provide relevant spectral information at the finest spatial resolution for the detection of charcoal sites. SWIR has a relatively low spatial resolution of 20m but it is used regularly for burnt area mapping thus tested in this study.

Table 2: Sentinel-2 spectral bands used for the study highlighted in **bold**

Sentinel-2 bands	Spatial resolution	Central wavelength (nm)	Bandwidth (nm)
Band 1 – Coastal aerosol	60	443	20
Band 2 – Blue	**10**	**490**	**65**
Band 3 – Green	**10**	**560**	**35**
Band 4 – Red	**10**	**665**	**30**
Band 5 – red edge	20	705	15
Band 6 –red edge	20	740	15
Band 7 –red edge	20	783	20
Band 8 – NIR	**10**	**842**	**115**
Band 8A – Narrow NIR	20	865	20
Band 9 – Water vapour	60	945	20
Band 10 – SWIR – Cirrus	60	1375	30
Band 11 – SWIR	**20**	**1610**	**90**
Band 12 – SWIR	**20**	**2190**	**180**

A total of 90 images of different dates since January 2016 until December 2018 were downloaded from the Copernicus Open Access Hub (Copernicus, 2017). The images are provided in tiles of 100x100km in "37MHV" in WGS_1984_UTM_Zone_37S coordinate system covering the area of interest. For the area of interest, all images were checked for cloud cover and all those that were at least 5% cloud free were used in the study. The images were downloaded as LC1 products, corresponding to Top-of-Atmosphere (TOA) reflectance. Atmospheric correction was performed to remove the atmospheric effects and obtain Bottom-of-Atmosphere (BOA) reflectance using the Sen2cor toolbox version 2.5.5 (ESA, 2018). In addition to atmospheric correction, Sen2cor generated a scene classification layer for each image that was used as a mask to remove clouds and cloud shadows from the images retaining dark area pixels, vegetation, bare soil, and water. The scene classification layer, SWIR1, and SWIR2 spectral bands were resampled from 20m to 10m spatial resolution to match the visible and NIR bands. Cloud masking was performed using an IDL code developed by Anton Vrieling purposely for Sentinel-2 data cloud masking and image stacking. In order to remove cloud shadows that could not be detected, a buffer of 50 meters around already masked pixels was used and all the cloudy pixels were given a code value of "-3001". The output was a temporal stack for each of the blue, green, red, NIR, SWIR1, and SWIR2 spectral bands clipped to the area of interest.

3. METHODS

3.1. Detection of charcoal production sites using VHR images

In order to accurately detect charcoal production sites on a VHR image, a semi-automated workflow was used, involving an automatic segmentation of the image and a manual selection of the charcoal site segments using visual interpretation. The latest WorldView-2 image (12 April 2018) was used for the segmentation to be able to trace back in time using the other VHR images and detect new sites that appear during the study period (Section 3.2). Figure 3 shows the AOI and a detailed view of the WorldView-2 image used for segmentation and detection of charcoal sites. The black circular objects on the image are the charcoal sites to be detected.

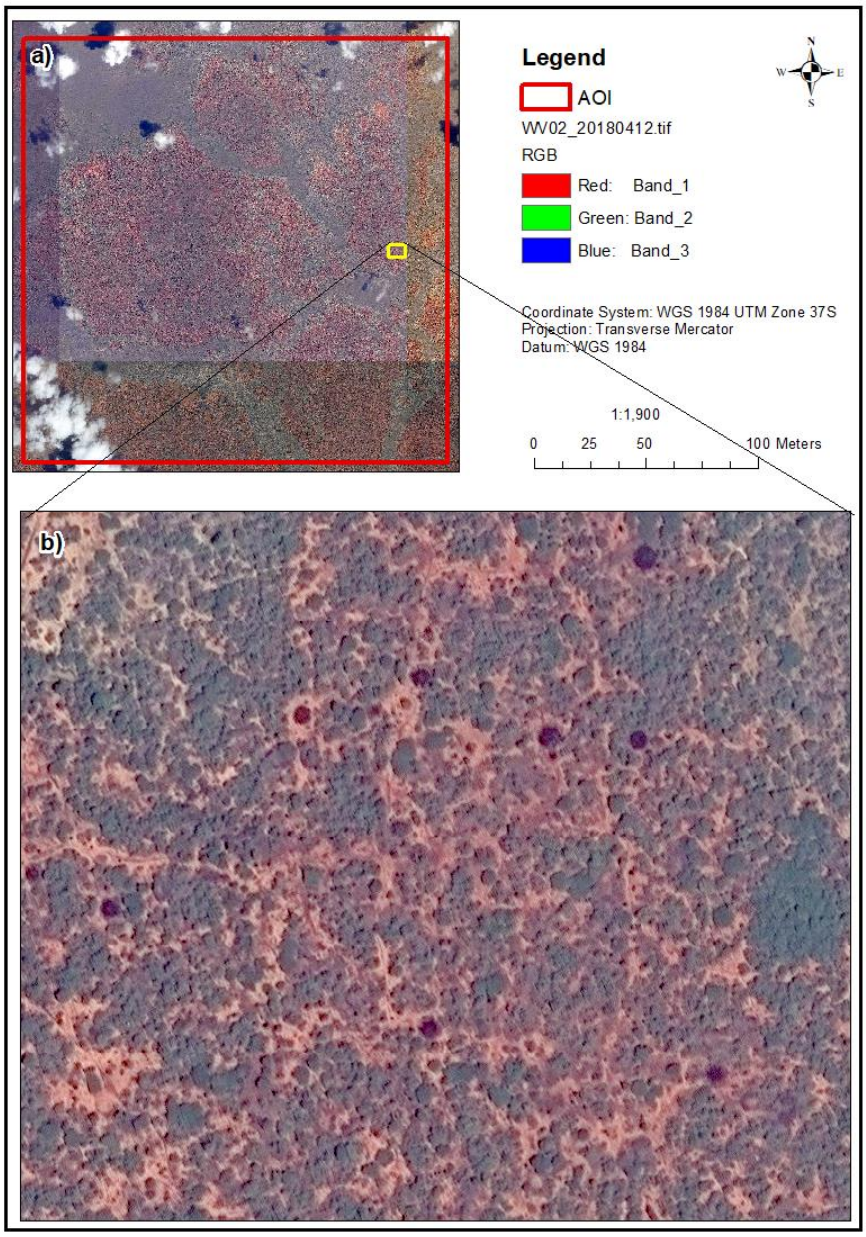

Figure 3: Charcoal sites as seen on 12 April, 2018: a) area of interest with the WorldView-2 image in the background and b) zoomed-in section of the image showing charcoal sites (black circular objects) to be detected

The image contained six tiles which were clipped to the AOI and segmented separately using the Orfeo Toolbox (OTB), an open source project for remote sensing images processing (OrfeoToolbox, 2016). The image segmentation function of OTB-6.6.0 was accessed and used through the command line. Mean-shift was used as the segmentation algorithm with spatial radius and range radius of 20 and 10 respectively. The result of the segmentation was a vector file in shapefile format with polygons of delineated objects on the image. The polygons were then overlaid on the image in ArcMap and through a visual interpretation, polygons that covered the black circular objects were manually selected and saved as charcoal sites (Figure 4). The shapefile was converted to WGS_1984_UTM_Zone_37S coordinate system the same as for Sentinel-2 images. A new column was added to the attribute table and the size (diameter in meters) was calculated based on the surface area of each polygon.

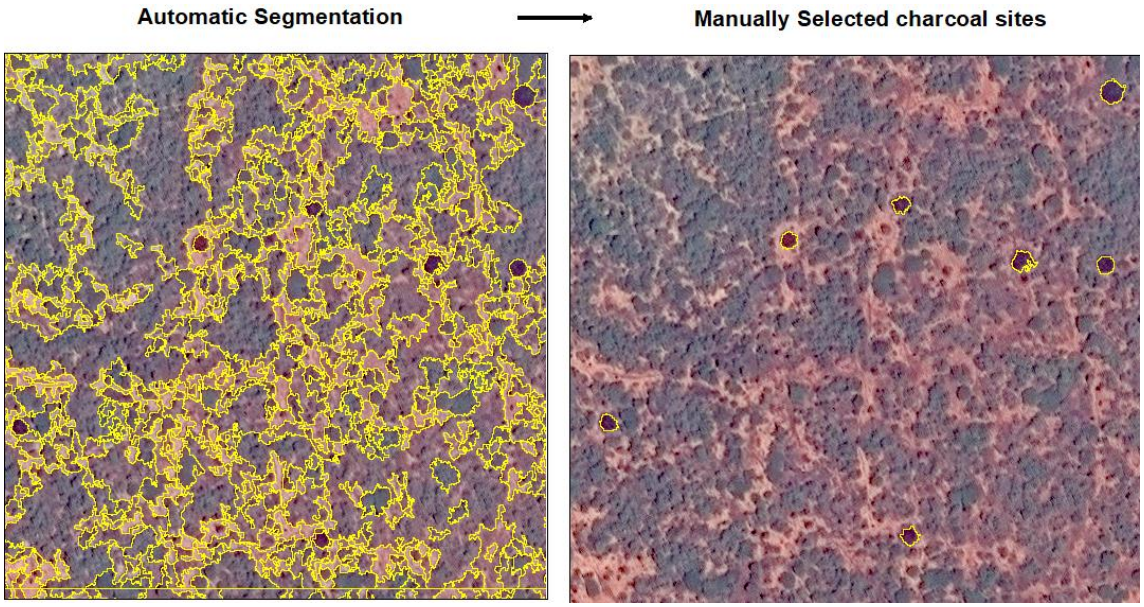

Figure 4: Semi-automated workflow for the detection of charcoal production sites on a VHR image: Automatic segmentation of the image (Left) and manual selection of charcoal segments (Right)

3.2. A detailed temporal analysis of the charcoal sites

To identify new sites that appeared during the study period, a temporal analysis for each charcoal site was carried out using all the VHR images obtained since August 2016. After the detection of sites on the 12 April 2018 image, a visual interpretation of all previous images was done to identify which of the identified sites appeared within the past two years and to understand with more temporal detail when they first appeared. Figure 5 shows the temporal stack of the VHR images used for this analysis.

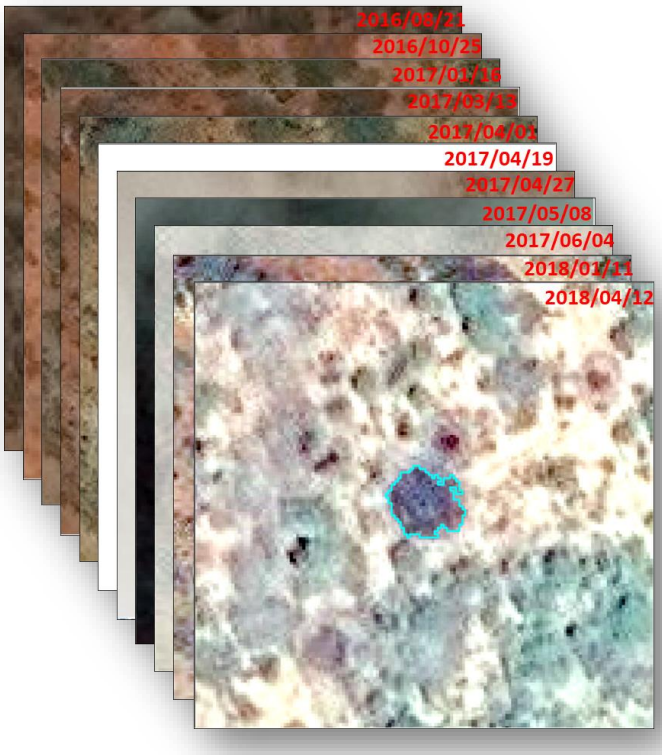

Figure 5: A temporal stack of the VHR images for one charcoal production site

All sites were overlaid on the images. Starting with the earliest image in time, each site was assessed to obtain information of its presence or absence in a particular image.

Steps were taken to complete the temporal profile for each site;

- Using ArcMap, 11 new columns were added to the attribute table of the charcoal sites (detected on 12 April 2018 image) to record information for each site and for each image date.
- For each site and date a code was entered, i.e. "-1" for cloudy/missing data, "0" for no visible evidence of charcoal site presence, and "1" for charcoal site presence

Figure 6 illustrates the temporal trajectory of one new site and how the table was populated with the three codes.

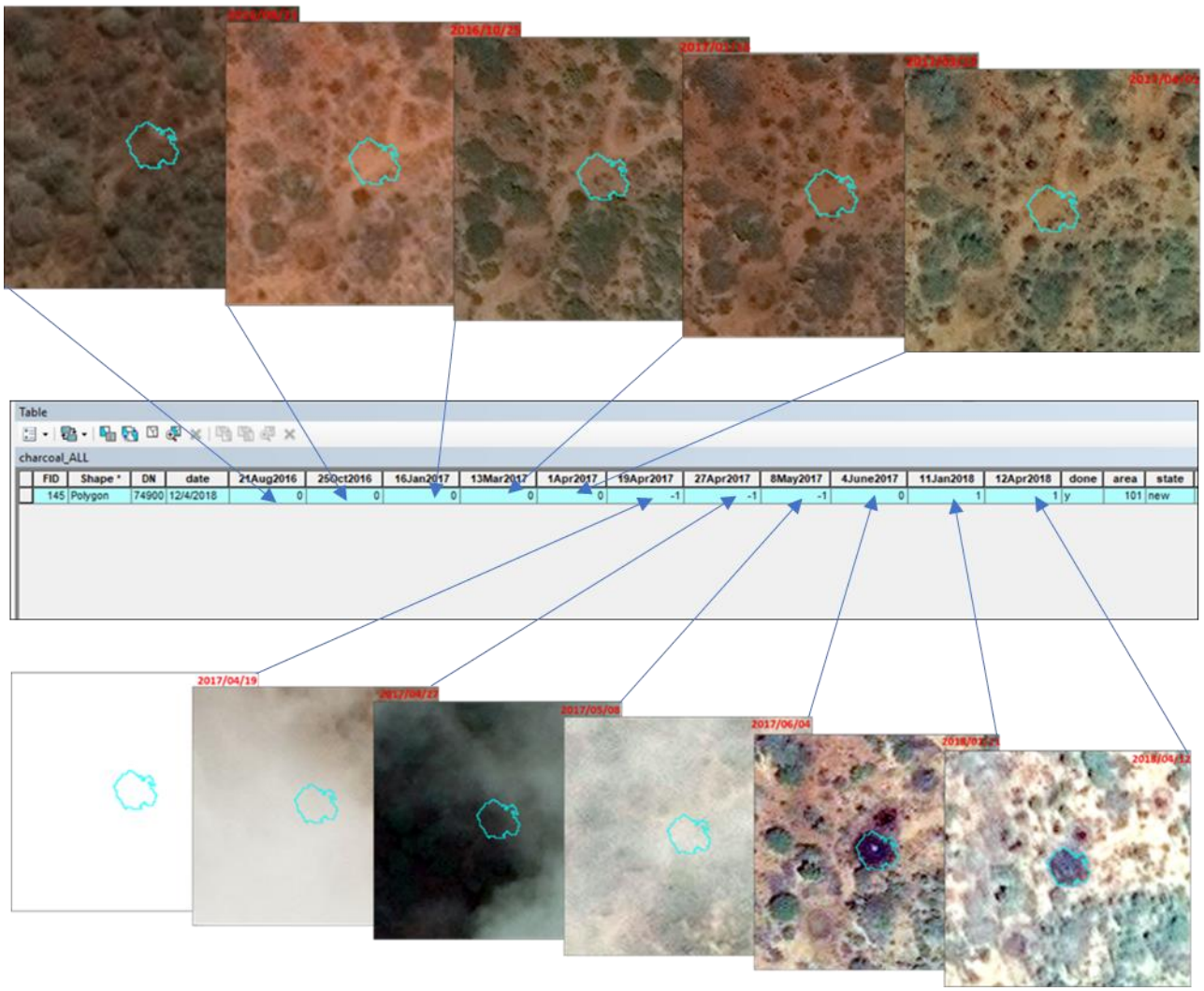

Figure 6: Analysis of the temporal trajectory for one charcoal site

For this particular site, the first evidence of its presence was on 11 January 2018 thus it was given code "1" for that particular date. For the earlier dates, the site is either not there ("0") or the images are clouded ("-1"). As a result, it can be inferred that this site has appeared between 4 June 2017 and 11 January 2018, which is the information that was used later when comparing against Sentinel-2 imagery.

3.3. Spatial and temporal variability of Sentinel-2 surface reflectance for charcoal sites

From the assessment with VHR and a visual interpretation, the charcoal sites were overlaid on Sentinel-2 multispectral image to check if their spectral signal would be strong enough to affect the Sentinel-2 reflectance. However, because sites are relatively small, a clear signal for most of the sites could not be detected. Therefore, to enhance the signal of charcoal sites from Sentinel-2 images, a combination of spatial and temporal characteristics was used to assess the changes in the reflectance of pixels. The reflectance of each pixel was compared with its surrounding by calculating a difference between them and assessed over time. It is expected that if a charcoal site appears, the reflectance of charcoal pixels will become significantly different from the surrounding pixels. Therefore, charcoal sites that appeared during the study period were considered and used to extract their pixel values from the Sentinel-2 images to detect changes in their reflectance over time.

3.3.1. Criteria for the selection of sample charcoal sites for the spatio-temporal assessment

A sample of the new charcoal sites that were obtained as described in Section 3.2, were converted from polygons into points and used for the assessment. As a sample, all sites were taken for which the timing of appearance could be determined to lie within a period of three months. Due to the big gaps in the VHR images due to clouds or missing images, the timing of appearance for some sites could not be determined with great detail. For example, if a site appeared between June 2017 and January 2018, it was not considered. The selected samples were later used to extract pixel values from the indices that were developed by assessing the centre pixel and its surrounding environment (Sub-section 3.3.2).

3.3.2. Assessment of the charcoal pixel with its surrounding environment

The Sentinel-2 temporal stacks generated for each spectral band as described in Sub-section 2.2.2 were used for this assessment. In accordance with the VHR assessment, most sites were at least 20m close to each other. Therefore, a window of 5x5 pixels was chosen to be the surrounding environment to avoid taking the charcoal signal of other sites as the surrounding if a larger window was considered. For each image date in a stack, an average value of each pixel and its neighbours in a window of 5x5 was computed. This value was assigned to the centre pixel within that window. This was achieved in R-programming language using the "Focal function", which is a spatial moving function to analyse the focal cell and its neighbourhood. Because a charcoal site may overlap multiple neighbouring pixels, the 3x3 window average value was also computed and subtracted from the 5x5 window value, and the result can be referred to as the "surrounding index". This implies that the surrounding index is the average of the pixels in the 5x5 window excluding the 3x3 window. After that, a difference between the original centre pixel value and the average of the surrounding pixels was computed, referred to as the "difference index". In order to avoid the effect of the cloudy pixels in these calculations, all pixels with values below zero (or -3001) were set to NULL before applying the Focal function. Figure 7 illustrates the general concept of calculating the difference index for one pixel.

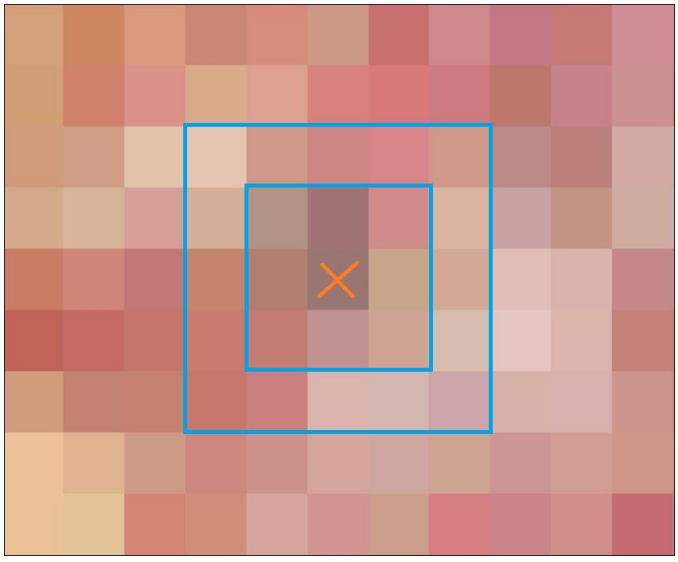

Figure 7: Illustration of the "difference index" concept for a single pixel on a Sentinel-2 false colour image: the pixel with an orange cross represents the centre pixel and the blue delineated pixels are the surrounding pixels.

In Figure 7, the value of centre pixel with a cross was subtracted from the average value of the blue delineated area to obtain the difference index values. To ensure equal weight while averaging all pixels in a window and avoid interference of cloud or shadow contamination when detecting sites, if any pixel in the specified window had a NULL value, the result of the central pixel was NULL. Therefore, to ensure the same for the original image before using it to compute the difference index, a "mask function" was used to calculate all pixels in the original image that were NULL in the surrounding index to NULL.

Using the selected charcoal sites samples, pixel values were then extracted from the original raster, surrounding index and the difference index using the "extract function" in R. The extracted values were then plotted over time to see if there was a significant difference in the values before and after the appearance of a particular charcoal site. This assessment was performed for the six selected spectral bands and the performance of each band in providing a clear charcoal signal was analysed. The selection was based on the band that provides a consistently higher change in difference after the appearance of a charcoal site. The selected band was then used for the extraction of a sample of non-charcoal pixels to compare their temporal trajectory with that of charcoal pixels. The difference in their behaviour was then used as a basis for the detection of charcoal sites.

3.4. Developing an automated Sentinel-2 based detection approach for charcoal sites

If the spatio-temporal characteristics of charcoal sites results in a significantly different temporal behaviour from that of non-charcoal sites (Sub-section 3.3.2), then an automated detection approach could be envisaged to detect charcoal sites from the Sentinel-2 time series. It is expected that when a charcoal site appears (i.e. when it is uncovered and charcoal remains and ashes create a dark circular object), there is a significant change in the spectral reflectance of the charcoal pixels and this change persists for some time. Based on this assumption, a classification rule was defined to separate charcoal from non-charcoal pixels using the difference index for the automatic detection of charcoal sites. When a charcoal site appears, the difference between the spectral reflectance of the charcoal pixel and its surrounding becomes greater than that during the period before appearance, thus resulting in a large change. This change in difference can be assessed by calculating the difference between 'difference indices' at two consecutive points in time, where the previous value point is subtracted from the current one. This would mean that the maximum value in the time series for each pixel could be the most significant change, which could indicate the appearance of a charcoal site. However, since large differences could also be caused by the presence of noise due to undetected clouds, moving windows were applied to filter out this noise and obtain a clearer temporal signal, which indicates a consistent change over a longer period. This helps to obtain clear, significant and consistent changes and remove most of the random noises. The moving windows applied included; 60, 90, 120 and 180 days using both average and median to aggregate the values in the window. To compute the "change-in-difference index" for each moving window, the difference between the average or median value in the window before was subtracted from that in the window after for each point in time. Due to big gaps in the data, a minimum of three observations were considered valid for each window to make sure that the calculated average or median has a sufficient statistical basis by not considering a single value which could be an outlier due to noise. In order to determine the optimal threshold value that can be used to separate charcoal from non-charcoal pixels, the selected charcoal sites (Sub-section 3.3.1) and an equal number of non-charcoal samples were considered for this analysis. Charcoal sites were grouped into five diameter classes to assess if the size of a charcoal site has an effect on the charcoal signal in Sentinel-2 data.

Using the selected samples for both charcoal and non-charcoal pixels, the maximum values in the times series were extracted from the change-in-difference index and used to determine the optimal threshold value to be used for the detection of charcoal sites. For all moving windows /models the distribution of charcoal values was compared with those of non-charcoal using boxplots to obtain a range of values that can provide an optimal separation between the two classes. The range of values was later used to determine the optimal threshold using sensitivity and specificity analysis with the "PresenceAbsence" package in R. For this analysis, charcoal was considered as present with code "1" and non-charcoal as absent with code "0". Sensitivity is the fraction of the charcoal pixels correctly identified as charcoal while specificity is the fraction of the non-charcoal pixels correctly identified as non-charcoal (Manel et al.,

2002). In order to use the PresenceAbsence package, the values have be in a scale between zero and one. Thus, the lowest and highest value of maximum values were scaled to zero and one respectively. The threshold values as determined using the boxplots were then tested for all models to determine one that maximises specificity since a large number of non-charcoal pixels are expected in the image thus ensures that most of them are correctly classified. After the analysis, these values were rescaled back to the original values and the optimal threshold was applied to the change-in-difference index to map potential charcoal sites in the study area.

In addition to the optimal threshold, pixels values of the visible charcoal sites on the NIR band of Sentinel-2 were extracted to obtain the charcoal signal range that was used as a second condition to improve the detection of charcoal sites. The two conditions were then used to produce the charcoal and non-charcoal map. For any pixel in the change-in-difference index that had a value equal or greater than the optimal threshold and a median value falling in the defined range of the charcoal signal at the point of the maximum value in a specified window of days after, was classified as charcoal otherwise non-charcoal. The second condition was added to reduce on misclassifications of many non-charcoal pixels as charcoal that had maximum values above the optimal threshold but were outside the defined charcoal signal range.

After the detection of sites with Sentinel-2, all new sites as detected with VHR were used to check how many of them have been accurately detected using the selected threshold. Since a number of neighbouring pixels could be affected by the charcoal signal due to positional inaccuracies, a buffer of 10m was applied around each charcoal point and the number of pixels that were correctly classified as charcoal based on Sentinel-2 was computed.

4. RESULTS

4.1. Charcoal sites detected using VHR imagery

A total of 1,740 charcoal sites with an average diameter size of 8m were detected in the study area. In Figure 8 , the background image is a natural colour WorldView-2 image of 12 April 2018 that was used to detect charcoal (yellow polygons). In Figure 8a, it is observed that sites are mostly concentrated in the brownish areas than in the greenish smooth areas of the images. The greenish areas are mostly shrublands with a very limited tree presence whereas the brownish areas are mostly bare soil covered with scattered trees.

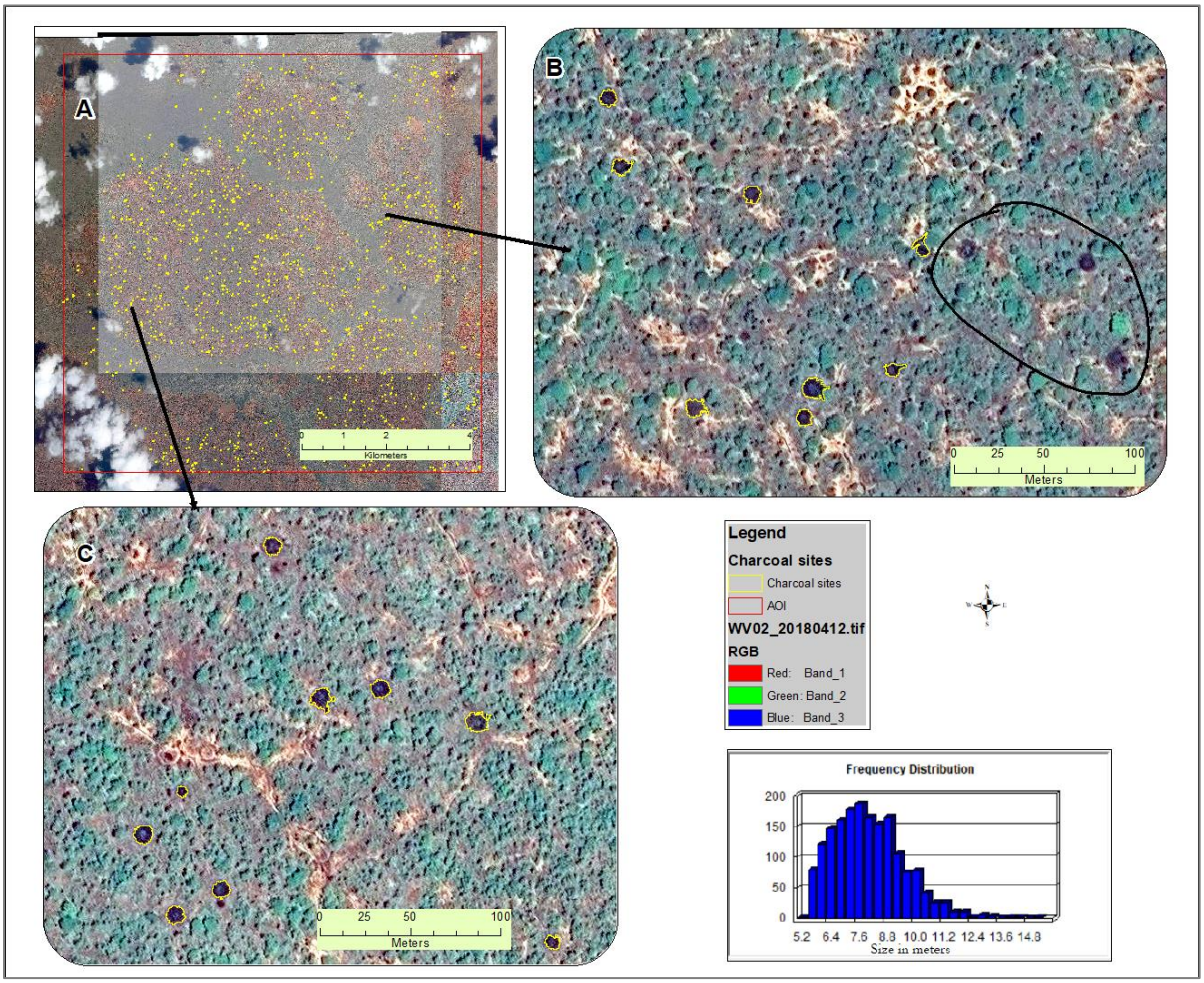

Figure 8: Location and distribution of charcoal production sites in the study area as detected on VHR image, 12th April 2018: a) overview of sites in the study area, b) a section of the study area with some sites that were not detected and c) a section of the study area where most sites even small ones were detected.

Most charcoal sites were accurately detected in the study area as it can be observed in Figure 8c. However, in some cases for example Figure 8b sites in a black circle were not detected.

4.2. Detailed temporal trajectory of the charcoal production sites based on VHR images

Out of the 1,740 detected charcoal sites, 439 were detected as new and 1,301 as old charcoal sites (Figure 9). New charcoal sites are as those sites that were not detected on the earlier VHR image (21 August 2016) but later in the study period whereas old sites are those sites that were detected on earlier image date. The size for both new and old sites is relatively the same with an average diameter of 8m.

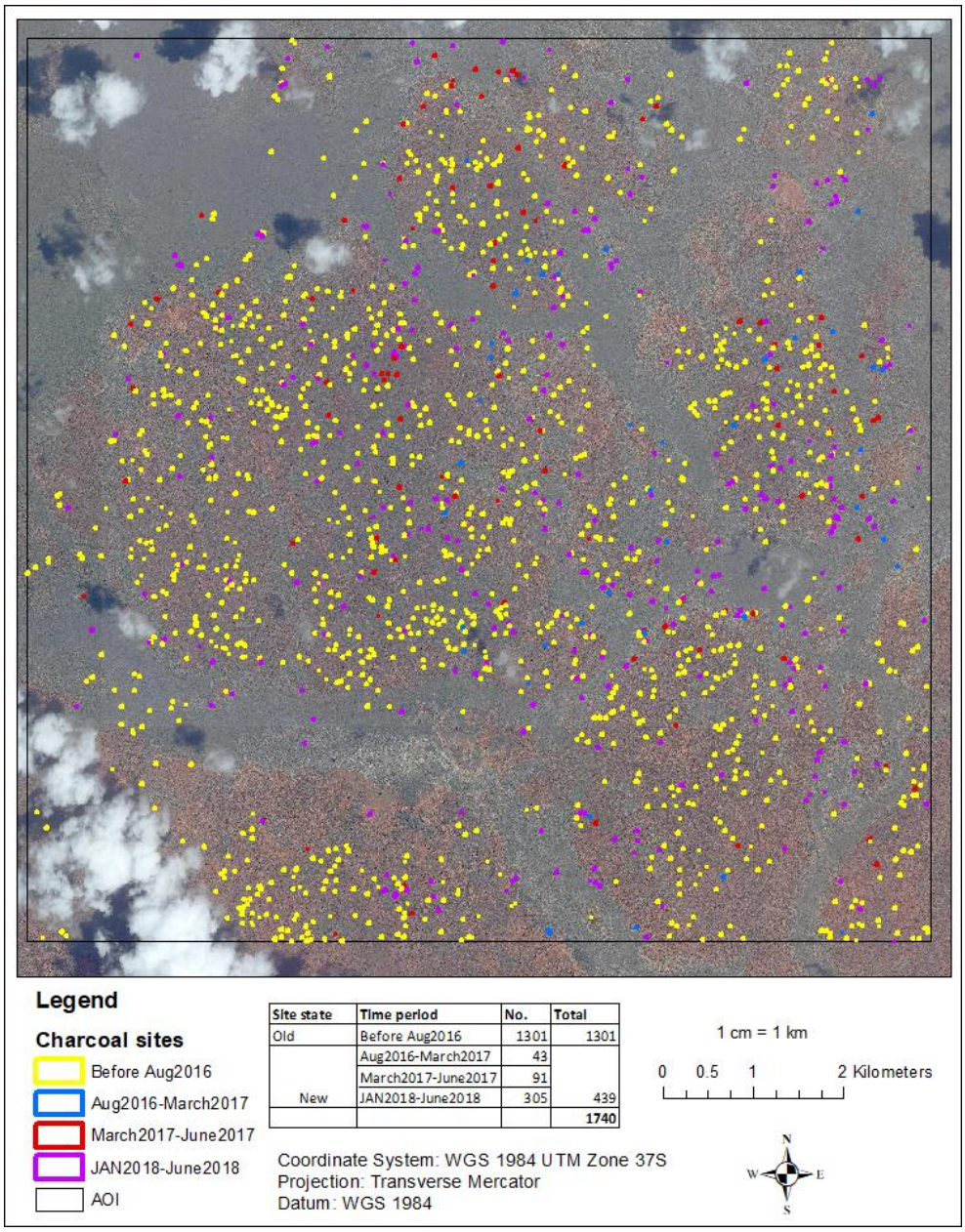

Figure 9: Location and distribution of old and new charcoal site in the study area based on their detection period

Visually, it can be observed in Figure 9 that there is no clear pattern in the spatial distribution of new and old sites in the study area, suggesting that within the area there is not a single clear 'frontier' of charcoal production that is moving in a specific direction. New sites are shown in three classes based on the detection time period and a large number of sites is observed in the time period of January 2018 to June 2018. However, it should be noted that these sites are classified considering the first appearance or detection date but there is a possibility that some sites could have appeared earlier but were not visible due to clouds or missing data.

4.3. The potential of Sentinel-2 to detect charcoal production sites

The new charcoal sites as detected with the VHR assessment were overlaid on Sentinel-2 images of the corresponding dates to see if the charcoal signal visually affects the Sentinel-2's reflectance. A selected number of sites were assessed and the results showed that for many of the sites, there was a clear difference in the reflectance of the charcoal pixels before and after the appearance of a site. Figure 10 shows three charcoal sites of different diameter sizes overlaid on two different Sentinel-2 false colour images of 10 September 2017 and 8 January 2018 which is the appearance period of these sites.

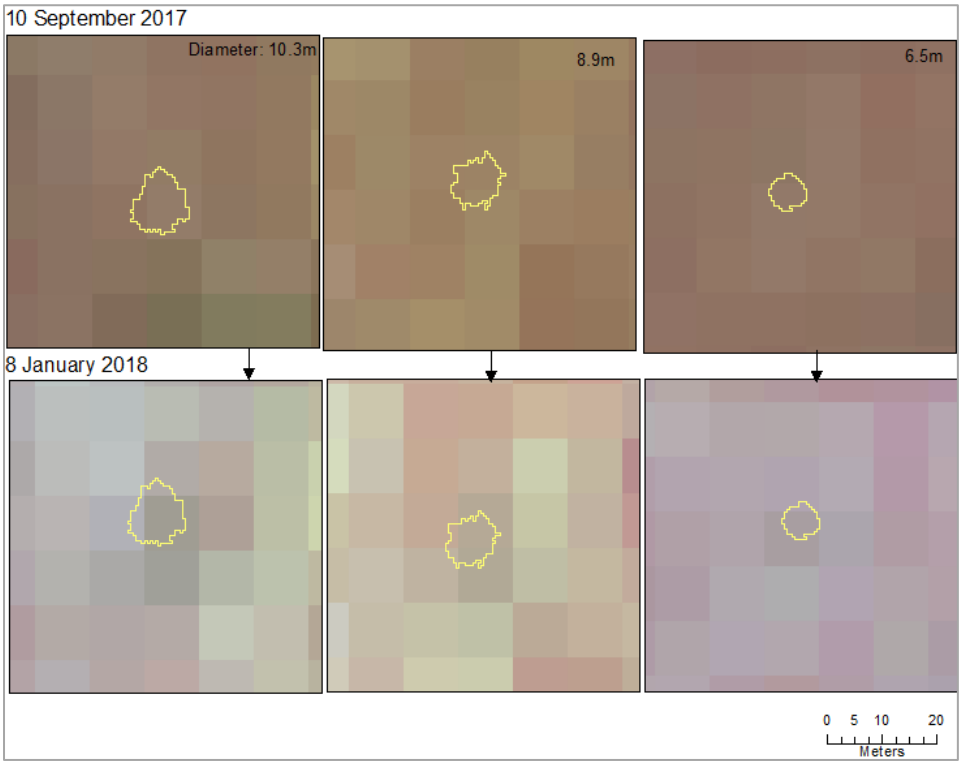

Figure 10: Two Sentinel-2 false colour images showing the reflectance of charcoal pixels before and after the appearance of three charcoal sites of different sizes.

Figure 10 shows that for the three sites, the charcoal signal of the charcoal site was not evident on 10 September 2017 with a very similar reflection as its surrounding. However, on 8 January 2018 when the charcoal sites appeared according to the VHR analysis, it is observed that the charcoal pixels became darker than their surroundings. Because exposed charcoal sites are black objects, they cause a drop or reduction in the visible and NIR reflectance thus making the pixels dark. It was observed, however, that for some smaller sites the signal was not strong enough to be detected visually. It was also observed that in some cases, there were shifts in the images whereby the charcoal polygon was not overlaying well with the charcoal pixels (Appendix 3). Therefore, accurate detection of sites is not feasible based solely on the reflectance of a single image, but rather a combination of spatial and temporal characteristics are required to assess the charcoal signal.

4.3.1. Assessment of the spectral reflectance of charcoal pixels and their surrounding

For this assessment, 162 out of the 439 new sites were used because the timing of appearance lied within a period of three months. The extracted pixel values from the original images, surrounding index and difference index were plotted over time. Figures 11 and 12 show the temporal behaviour of two selected charcoal pixels for all the spectral bands used for the study. The centre pixel (blue) line represents the original reflectance of the centre pixel, surrounding (green) represents the average reflectance of the surrounding pixels, and difference (red) represents the difference between the centre pixel and its

surrounding. The black dotted vertical lines show the appearance period of the charcoal site as detected with VHR times series.

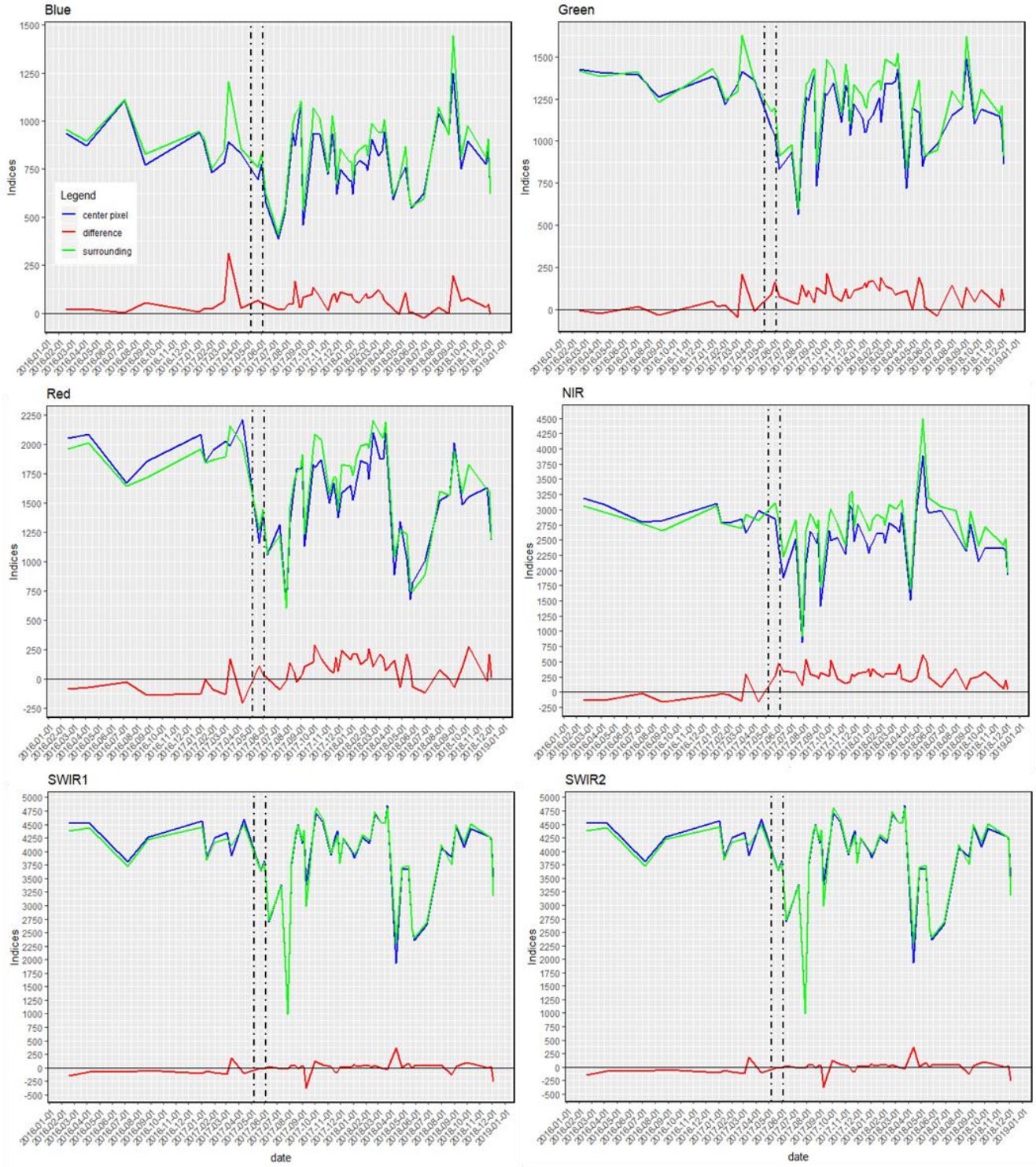

Figure 11: Temporal surface reflectance profile of a charcoal site (8m diameter) for each selected spectral bands of Sentinel-2. The black dotted vertical line represent the appearance period of the site.

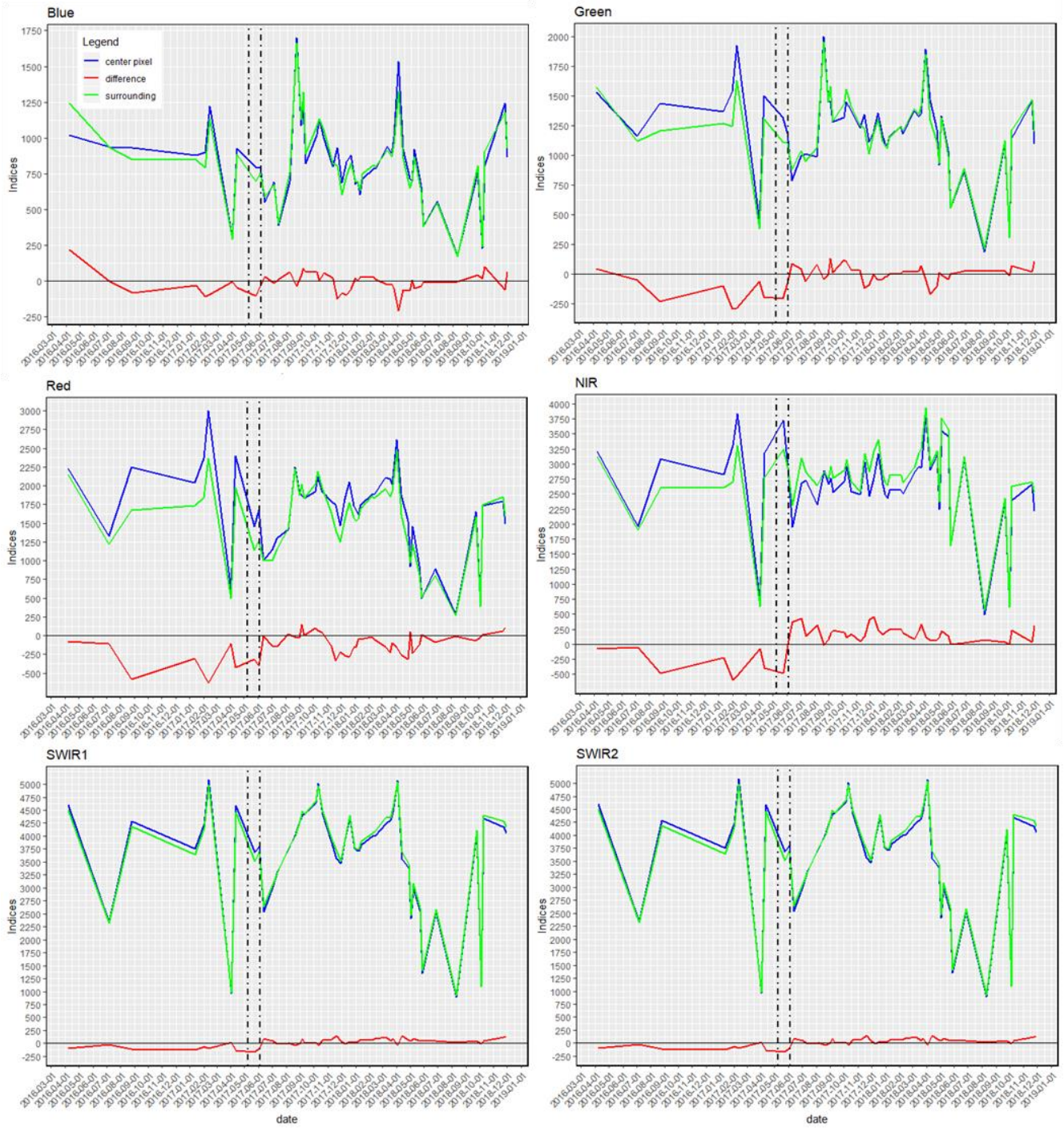

Figure 12: Temporal surface reflectance profile of a charcoal site (9m diameter) for each selected spectral bands of Sentinel-2. The black dotted vertical line represent the appearance period of the site.

For the green, red and NIR bands, it is observed that the difference between the centre pixel and its surrounding increases during the appearance period of the charcoal site. For the blue, SWIR1 and SWIR2, there is no clear observed difference in the reflectance before and after the appearance of the sites. This implies that the appearance of a charcoal kiln results in a clear change in the difference index but the signal is stronger in some spectral bands than in others.

4.3.2. Selection of the spectral band to consider for the detection of charcoal sites.

In order to select the most promising band in term of providing a consistently higher change in difference, six sites of different diameter sizes were used, their values extracted from the difference index and plotted over time for all spectral bands (Figure 13).

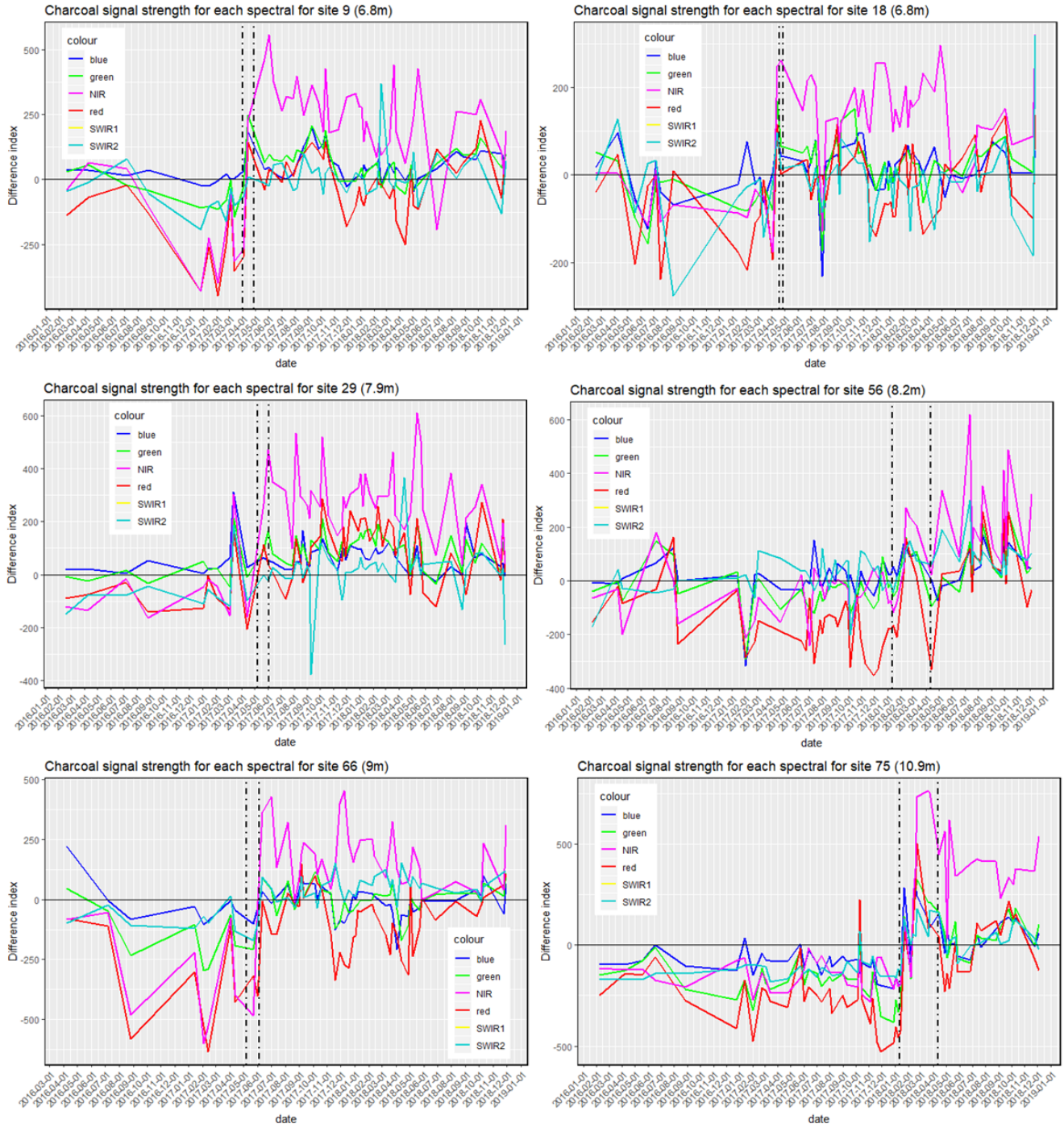

Figure 13:Temporal trajectory plots of six charcoal sites of different diameter sizes showing the performance of each spectral band in terms of providing a stronger charcoal signal after the appearance of a site

Figure 13 shows that NIR performs better than the other bands with a constant larger and seemingly more consistent change in the difference index after the appearance of the charcoal sites. This was the case for some of the sites as shown in Appendix 1 but not for all, Appendix 2. Therefore, since NIR bands performed better than other bands, it was used for the rest of the analysis in this study.

4.3.3. Comparison of the charcoal site temporal trajectory with the non-charcoal pixels using NIR difference index

The difference index was plotted over time for a number of non-charcoal pixels to see if the temporal trajectory would be different from that of the charcoal sites (Figure 14). The figure shows the trends of six randomly selected non-charcoal pixels.

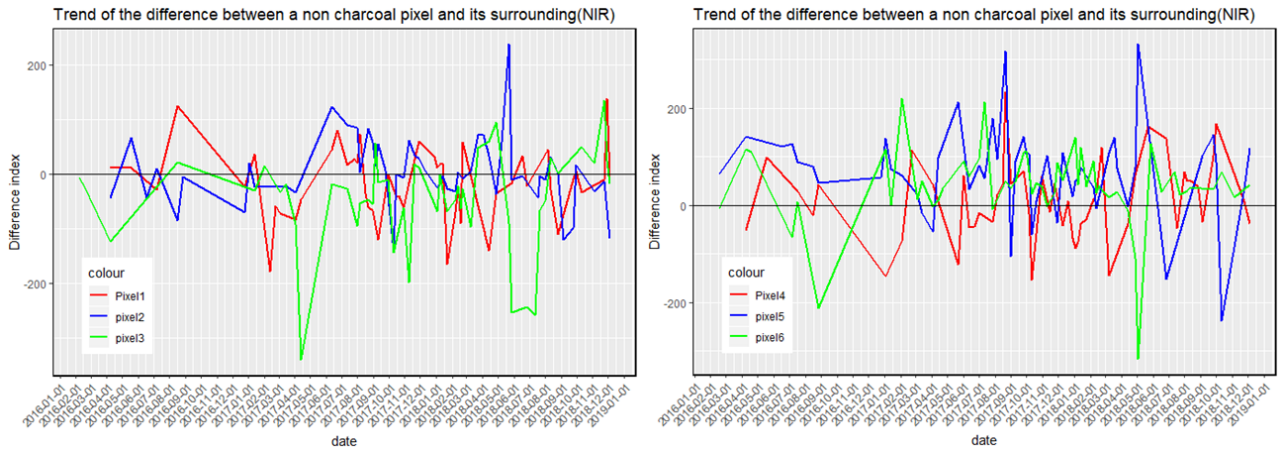

Figure 14: Plots showing the temporal trajectories of six non-charcoal pixels

For none of the six non-charcoal pixels, a significant change in difference between the centre pixel was observed. Despite the limited sample, the temporal analysis of the difference index provides a basis for the separation of the two classes for the detection of charcoal sites in the study area.

4.4. Automation of the detection of charcoal production sites

4.4.1. Selection of the optimal moving window and threshold

The change-in-difference index was computed as described in Section 3.4 and the maximum values of 162 samples for charcoal and non-charcoal pixels were obtained. Figure 15 shows the distribution of the maximum values for charcoal and non-charcoal pixels for each moving window.

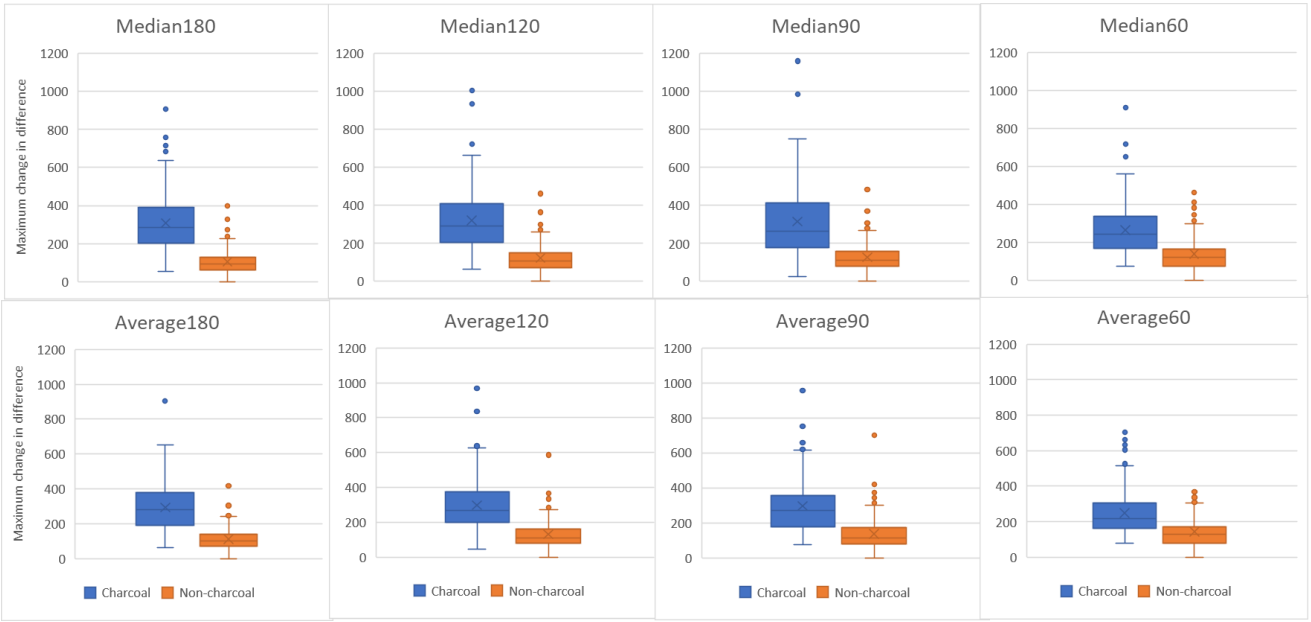

Figure 15: Box plots showing the distribution of the maximum change in difference values for charcoal and non-charcoal pixels for each moving window

It can be observed in Figure 15 that the values of charcoal pixels for all moving windows are relatively higher than those of the non-charcoal pixels. This indicates that for most of the charcoal pixels, the signal was strong enough to provide a large change in difference at the points of their appearance. However, it is observed that a substantial overlap exists between the index values for charcoal and non-charcoal sites. Therefore a number of index values were used to determine the optimal moving window and threshold that gives very little confusion between charcoal and non-charcoal (Figure 16).

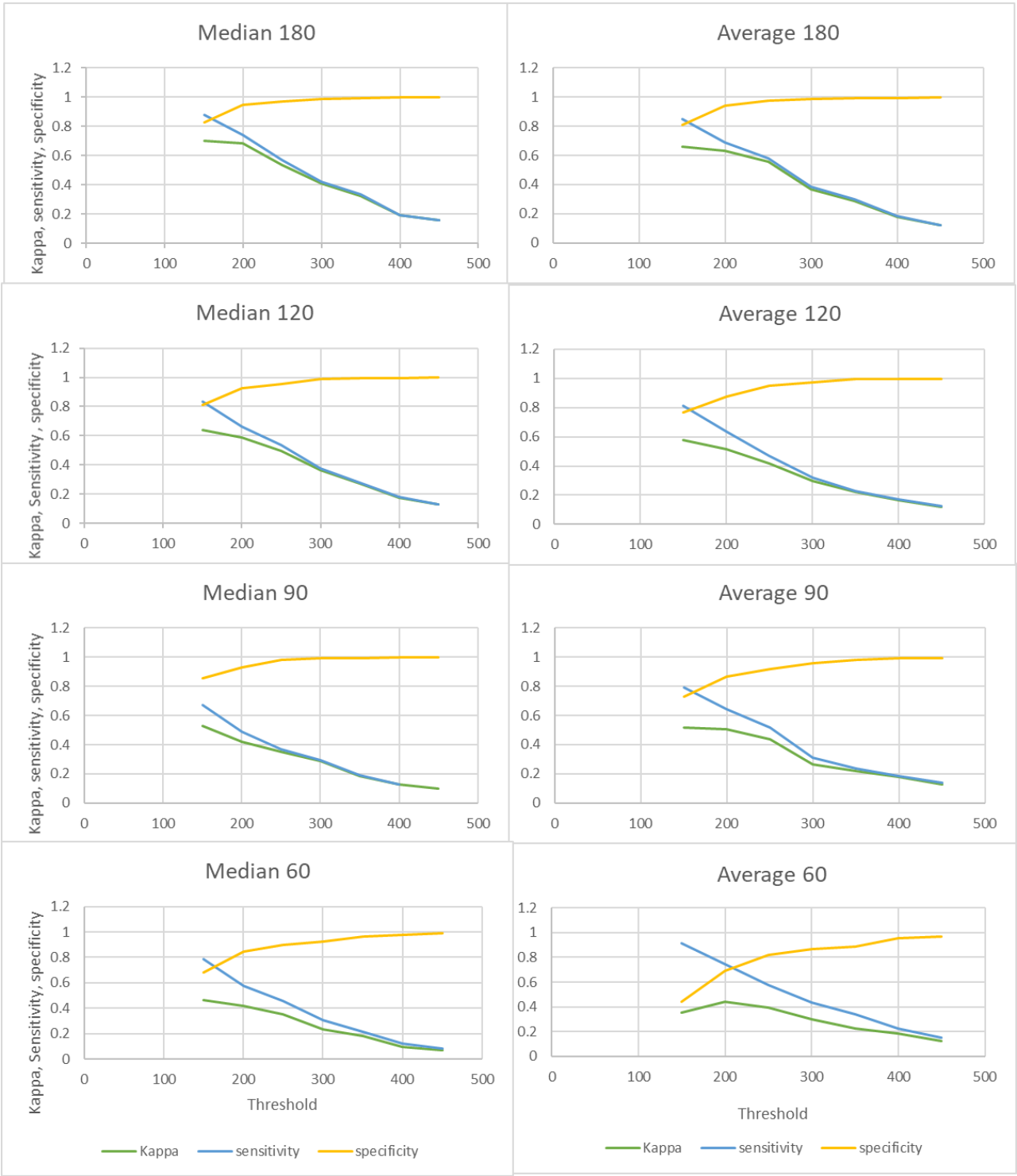

Figure 16: Line graphs showing the Kappa, sensitivity and specificity values at different thresholds for all moving windows

Figure 16 shows that for all thresholds, the 180 days moving median and average have the highest kappa values implying best performing moving window. This can be explained by the fact that a longer time window accounts better for the noise, which for the shorter windows result more often in misclassifications. Therefore, a 180 days moving window was considered to be the optimal model that was used to determine the optimal threshold by comparing the sensitivity, specificity and kappa values of all thresholds. For the purposes of maximising specificity and reducing confusion between the two classes, thresholds such as 300 and above give up to 100% specificity but threshold 400 seems to provide an optimal detection of charcoal sites. Threshold 400 has a sensitivity of 19% which substantially reduces the misclassification of non-charcoal pixels as charcoal as compared to other thresholds.

4.4.2. Detectability of charcoal sites based on their diameter size

It is expected that larger sites might be easier to be detected as compared to smaller sites, therefore it was important to assess if the size of a charcoal site has an effect on its detectability. The charcoal sites were divided into five diameter classes as described in Section 3.4 and Figure 17 shows the relationship between the maximum change in difference and the diameter classes. It can be observed that charcoal sites with diameters between 5m and 8m have relatively lower change in difference as compared to the bigger sites of 8m and above, but the relationship as expected is not very strong.

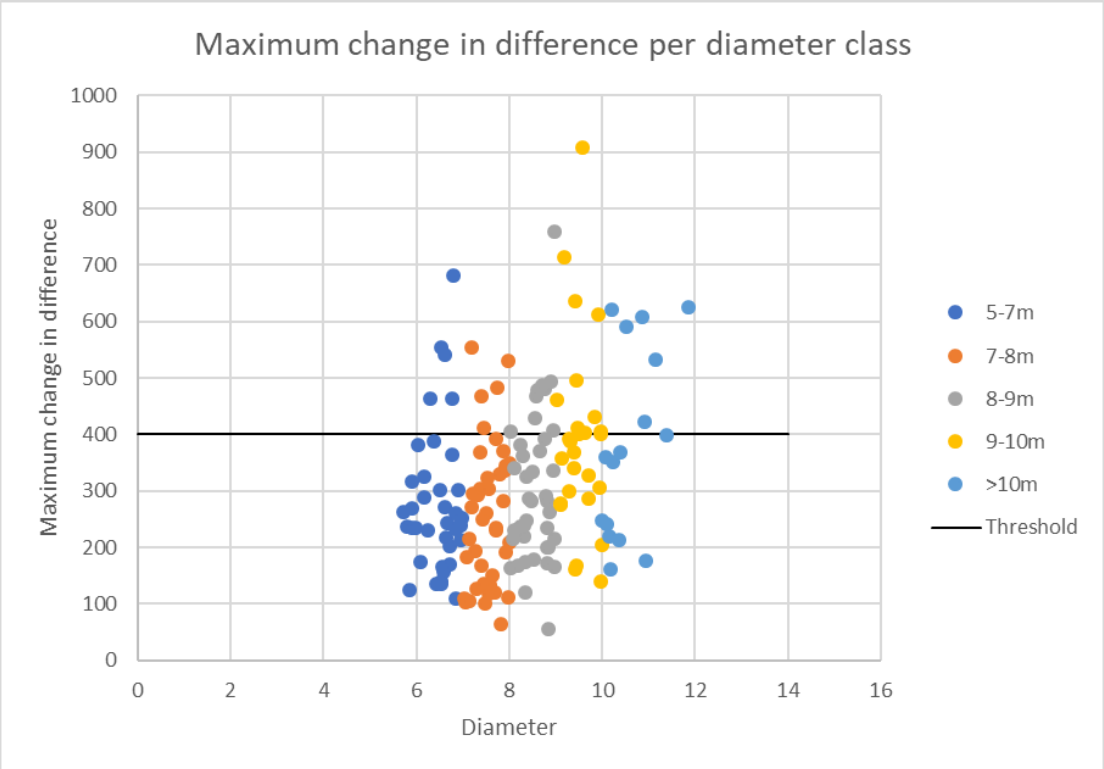

Figure 17: A scatter plot showing detectability of charcoal sites depending on their diameter size

Considering the threshold of 400 as the optimal indicated by the black horizontal line on Figure 17, the percentage of charcoal sites that can be detected per class are shown in Table 3.

Table 3: Detectability percentage of charcoal site per diameter class

Diameter class	5-7m	7-8m	8-9m	9-10m	>10m	Total
No. of sites	38	41	40	27	16	162
No. of sites > 400	5	5	7	8	6	31
Percentage (%)	13.2	12.2	17.5	29.6	37.5	19.1

The results in Table 3 indicate that for sites with a diameter larger than 8m, have a relatively higher percentage of being retrieved as compared those smaller than 8m. Therefore the size of a charcoal site has some influence on its detectability.

4.4.3. Mapping of charcoal sites on sentinel-2 image

In addition to the optimal threshold, a range of NIR reflectance values of the charcoal signal was used for the detection of charcoal sites in the study area. Examination of the NIR reflectance of the visible charcoal sites (centre pixel) indicates that their reflectance range between 0.18 and 0.25 based on sample pixels. Therefore, if a pixel had a change in difference value above the optimal threshold and a median reflectance of 0.18-0.25 for the 180 days after the maximum change-in-difference index, was classified as charcoal else non-charcoal. Based on Figure 16, thresholds 300, 350, 400 and 450 provided a specificity close to 100% thus used for the detection of charcoal sites and Figure 18 shows the number of pixels that are correctly classified as charcoal per threshold.

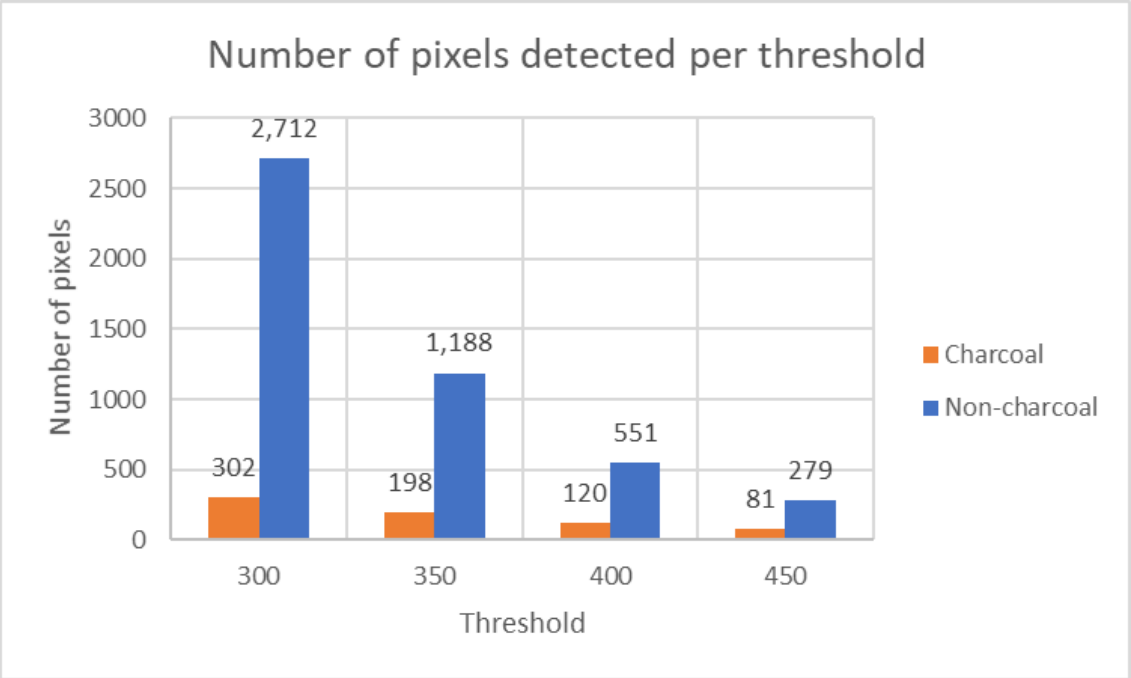

Figure 18: A bar graph showing the number of pixels detected as charcoal and non-charcoal per threshold

Figure 18 shows that the lower the threshold, the more non-charcoal pixel classified as charcoal. Increasing the threshold means reducing misclassifications but it also reduces the number of charcoal pixels correctly classified as charcoal. Therefore, 400 gives the optimal classification of charcoal and non-charcoal pixels in this study. The spatial representation of the detection with the 400 threshold is shown in Figure 19.

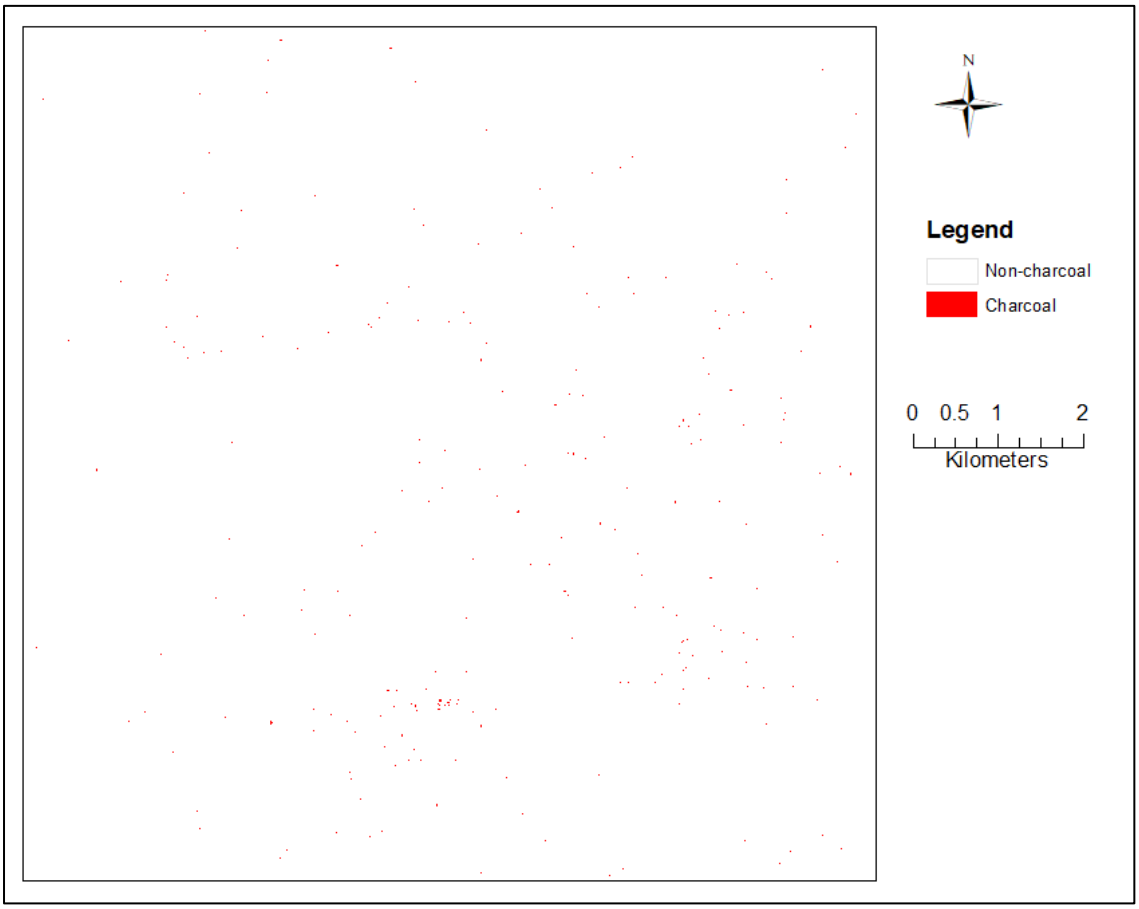

Figure 19: A map showing charcoal sites detected at a threshold of 400 change-in-difference index based on Sentinel-2 time series.

Figure 19 shows the pixels detected as charcoal in red and in total they are 671 out of which only 120 are actual charcoal sites are detected with VHR. Figure 20 shows a temporal trajectory of a sample of six non-charcoal pixels that were misclassified as charcoal.

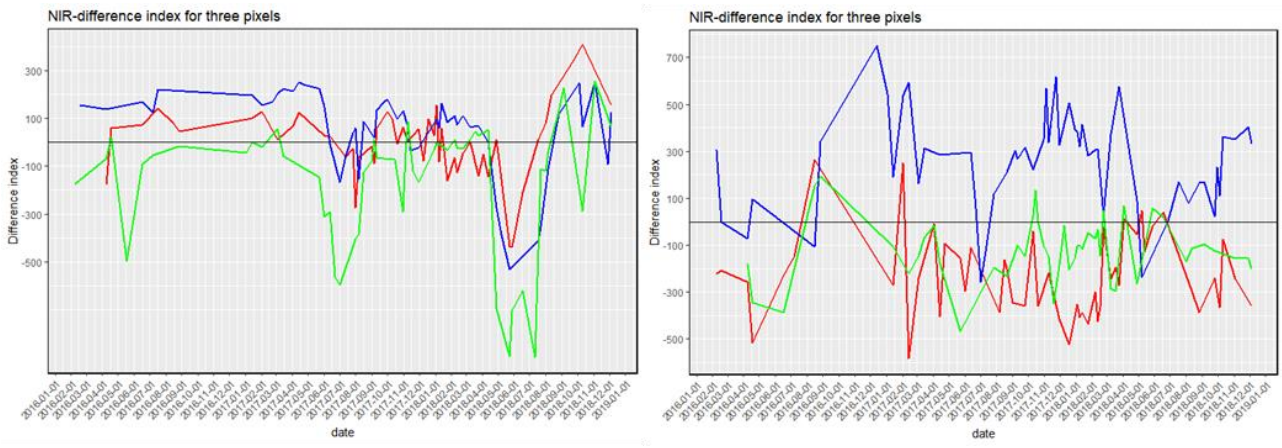

Figure 20: Temporal trajectories of six non-charcoal pixels misclassified as charcoal

It is observed in Figure 20 that the trajectory of these pixels is not similar to that of the charcoal pixels (Figure 11 &12) but a lot of noise is observed which could have led to the large change in difference thus their detection as charcoal sites.

5. DISCUSSION

5.1. Detection of charcoal sites on VHR image

For the segmentation of the image, Orfeo Toolbox (OTB) was successfully used and charcoal sites were clearly delineated with at least 95% the of sites detected in the study area. However, the segmentation process was very slow when it came to dealing with larger areas. To make the process faster, the study area was divided into four squares of 5x5km which were used to clip images before using OTB for segmentation. The four resulting vector files were then merged back to have a single shapefile of charcoal sites.

Segments of visible charcoal sites were manually selected but it took quite a long time to complete the entire 10x10km and it was also subject to errors where some sites could be missed. Therefore for an efficient approach that can be implemented over larger areas, automatic object-based classification using machine learning classifiers such as Random Forest (RF) or Support Vector Machines (SVM) could be explored for future studies (Cheng & Han, 2016).

A total of 1,740 charcoal sites were detected in the study area and it was found that charcoal sites were mostly located in areas covered with scattered trees and bare soil seen with brownish colour on the VHR image (Figure 8). This confirms that charcoal production is selectively carried out in tree-covered areas for high production as opposed to shrub areas (Bolognesi & Leonardi, 2018).

Bolognesi and Leonardi (2018) found out that the average diameter of charcoal sites is 6m, but this study obtained a larger average diameter of 8m. The reason for this difference could be due to the fact that for their study, charcoal sites were manually detected by drawing circles around them leading to improper delineation thus resulting in an underestimation of the average kiln size. Opposed to that, the automatic detection used in this study resulted in a proper and accurate delineation of the sites. Another possible reason for the difference could be because their study covered a larger study area (37,000 km2) with many charcoal sites and varying diameter sizes whereas this study worked in a 10x10km area.

5.2. Temporal trajectory of charcoal sites using VHR images

The temporal profile of each charcoal site was performed by manually checking the presence or absence of the site on all VHR images based on sites as detected on the April 2018 image. The process took a long time but given a small area of 10x10km, the manual approach was successful for this study. However, if a larger area would be considered, then this approach cannot be efficient. In this case, it will require automatic detection of charcoal sites in all images and track the presence or absence of sites in each image which could be possible with machine learning approaches.

During the temporal analysis, it was observed that the charcoal sites were not aligning well in all images indicating a shift in the images. In relation to the April 2018 image, other VHR images were shifted predominantly to the east with at most 10m. To handle the shift, any site that was visible in a subsequent image within 10m distance was assumed to be the same site. Ideas to automatically correct for the shift, such as image co-registration are available but given the fact that the process was manually done, they were not performed for this study.

From the temporal analysis, new sites were detected and it was observed that they were fewer than old sites. This could be because trees have reduced thus the reduction in charcoal production in the study

area. Another reason could be that old sites remain visible for a period longer than that of the new sites detected thus their large number. It should also be noted that there was no observed evidence of multiple use of the same sites. Based on expert knowledge at SWALIM, it is rare to find cases of reuses of the same site in a short period of time.

It was observed that a higher number of new sites were detected during the period of January 2018 to April 2018 which would confirm that charcoal production happens during this dry season based on expert knowledge at SWALIM. However, it should be noted that for this study the new sites were classified considering the first detection date but there is a possibility that some sites could have appeared earlier but not visible. This is because of the missing data and clouds most especially in the period before January 2018.

Bolognesi and Leonardi (2018) reported a change in kiln size in 2017 as compared to years before which they attributed to the reduction of larger trees due to charcoal production, gradually resulting in smaller charcoal kilns due to reduced wood availability. However, for this study, there was no significant diameter difference between new and old sites. This could be due to the shorter study period (2016-2018) that this study used as compared to their study (2011-2017).

5.3. Assessment of the surface reflectance of Sentinel-2 over time

Temporal analysis of Sentinel-2 images, particularly by assessing the reflectance of each pixel in relation to neighbouring pixels, proved to result in a reasonably clear signal for detecting charcoal production sites. For most of the charcoal pixels, there was a substantial increase in difference in the period of appearance of the charcoal site as analysed with VHR. This was the expected trajectory of a charcoal pixel which indicates that when the charcoal site appears, the surface reflectance of the centre pixel quickly reduces, which makes the pixel different from the surrounding environment. It should, however, be noted that not for all charcoal sites such a clear signal could be observed (Appendix 2)

Among all spectral bands of Sentinel-2 that were tested, NIR performed better in terms of providing a larger and more consistent change in difference after the appearance of a charcoal site. This result corresponds with Huang et al. (2016) who found out that NIR and SWIR bands of Sentinel-2 provided the strongest separation between burned and unburned areas as compared to other spectral bands, especially in the visible range. SWIR bands have been extensively used for burned area mapping, however, for this study, it did not yield good results probably due to a relatively coarser spatial resolution of 20m. Ideas to increase the spatial resolution have been proposed such as pan-sharpening of the SWIR bands of Sentinel-2 imagery (Park et al., 2017; Kaplan & Avdan, 2018), but they were not explored for this study due to the limitation of time.

5.4. Detection of charcoal sites using Sentinel-2 timeseries

The difference in the temporal trajectories of the charcoal and non-charcoal pixels was used as a basis for the separation of the two classes. This involved the computation of the change in difference over time and the results showed that the maximum values of charcoal pixels were relatively higher than those of the non-charcoal pixels. However, there were substantial overlaps between the two classes where non-charcoal pixels had high values as compared to some charcoal pixels. It was observed that noise due to the undetected clouds and cloud shadows greatly contributed to the high maximum values for both charcoal and non-charcoal pixels. Through a visual analysis, it was found out that the large values for non-charcoal pixels resulted when a low value due to noise at a given date was subtracted from a high actual value at the subsequent date. Some of the charcoal pixels were also affected in the same because it was observed that

the maximum change in difference values did not fall in the right appearance periods based on the VHR analysis. To reduce the noise effect moving windows of 60, 90, 120 and 180 days to aggregate data by average and median were used. The results show that the 180 days moving window performs better with the highest kappa values and minimal overlaps between the two classes. This could be due to the fact that a longer time period contains more observations thus is more effective in smoothing out noise in the data. In addition, the moving median performs better than the average due to the fact that the median is less sensitive to outliers.

Using the 180 days moving median for the detection of charcoal sites, thresholds based on the maximum change-in-difference index and NIR reflectance (0.18-0.25) were used. Thresholds 300, 350, 400 and 450 provided a specificity close to 100% but 400 (0.04 surface reflectance) was taken to be the most optimal one since less of the non-charcoal pixels were misclassified as charcoal while correctly classifying a significant number of charcoal pixels.

For this study, the thresholds were used separately because after applying the first one based on the change-in-difference index, it was observed that many non-charcoal sites were misclassified as charcoal. The addition of the second condition based on the NIR reflectance of the visible charcoal sites was used to reduce the misclassification and improve the detection result. However, future studies should consider combining this information in one index to obtain one optimal threshold to be applied to the entire image. Also, further assessment of the NIR reflectance values of the charcoal signal for a wider of range environmental conditions is required.

It was assumed that the size of charcoal sites would have an effect on their detectability, but results proved otherwise. Although charcoal sites above 8m diameter had a better representation of high maximum values than those below, the link was not strong enough to conclude that bigger sites have a stronger signal which makes them easily detectable. This could be due to the fact the charcoal signal may be captured in multiple neighbouring pixels thus the strength is similar for both small and big sites.

Despite remaining difficulties, this study has shown that Sentinel-2 has the potential for detecting small charcoal sites, even for sites smaller than sensor's spatial resolution. To obtain better results, listed are some of the challenges and possible solutions for further research.

- Given the approach used in this study to detect charcoal sites, noise due to clouds and cloud shadows in the Sentinel-2 data is the major factor hindering the accurate detection of charcoal sites. Therefore, in order to obtain better results, the cloud masking process should be improved to ensure that most of the noise is removed from the data but also other approaches such as BFAST for analysing the temporal trajectory to obtain significant change points in the data can be explored.
- A shift was observed with the different Sentinel-2 image dates where the charcoal signal was not constantly in the same location for all images. The signal was observed to change between the four neighbouring pixels (Appendix 4). For this study, a single (centre) pixel was considered but for future, research an approach to consider a pixel with the minimum value (stronger charcoal signals) within a 3x3 window could be developed.
- Different surrounding environments could also have an impact on the charcoal signal due to contrast. For example if a site is located on dark soils, the difference in the reflection will not be that large when a charcoal site appears thus making it difficult to be detected. For this study it was not explored but based on the method used, it could hinder the detection of some sites.

- The consideration of a 5x5 window in the computation of the surrounding index could have affected the detection of some sites. Through visual analysis, it was observed that at least 5% of sites were close to each in a distance of up to 20m thus the signal of one charcoal signal was computed in the surrounding of another site resulting in a small difference.
- For this study, NIR was used alone for the detection charcoal of sites but future study could use, machine learning algorithms such as RF and SVM to determine which spectral bands, their combinations or indices that can work best for the separation of the two classes. To further improve the detection results, land cover classification of the study area could also be used as input to eliminate sites detected in areas such as shrubs where charcoal production does not take place.

6. CONCLUSION

This study showed that the analysis of changes in near-infrared reflection at and around charcoal production sites allows to separate a specific signal, promising for automatic detection of such sites. Despite that the charcoal sites' diameters are generally smaller than the spatial resolution of the Sentinel-2 multispectral sensor, this study demonstrates their detection is possible. However, due to challenges such as clouds and big data gaps in the Sentinel-2 time series, accurate detection of charcoal sites was hindered. Future studies may improve the detection accuracy of charcoal production sites by further exploring the combined use of multiple spectral bands, as well as using machine learning algorithms.

LIST OF REFERENCES

Adams, J. B., Sabol, D. E., Kapos, V., Almeida Filho, R., Roberts, D. A., Smith, M. O., & Gillespie, A. R. (1995). Classification of multispectral images based on fractions of endmembers: Application to land-cover change in the Brazilian Amazon. *Remote Sensing of Environment*, *52*(2), 137–154. https://doi.org/10.1016/0034-4257(94)00098-8

Bolognesi, M., & Leonardi, U. (2018). *Analysis of very high-resolution satellite images to generate information on the charcoal production and its dynamics in South Somalia from 2011 to 2017. Technical Project Report. FAO-SWALIM, Nairobi, Kenya.* https://doi.org/10.13140/RG.2.2.22600.83203

Bolognesi, M., Vrieling, A., Rembold, F., & Gadain, H. (2015). Rapid mapping and impact estimation of illegal charcoal production in southern Somalia based on WorldView-1 imagery. *Energy for Sustainable Development*, *25*, 40–49. https://doi.org/10.1016/j.esd.2014.12.008

Brown, A. (2013). *Breaking the cycle of charcoal production in Somalia*. Mogadishu.

Cheng, G., & Han, J. (2016). A survey on object detection in optical remote sensing images. *ISPRS Journal of Photogrammetry and Remote Sensing*, *117*, 11–28. https://doi.org/10.1016/J.ISPRSJPRS.2016.03.014

Chidumayo, E. N., & Gumbo, D. J. (2013). The environmental impacts of charcoal production in tropical ecosystems of the world: A synthesis. *Energy for Sustainable Development*, *17*(2), 86–94. https://doi.org/10.1016/j.esd.2012.07.004

Climate-Data. (2017). Chisimayu climate: Average Temperature, weather by month, Chisimayu weather averages - Climate-Data.org. Retrieved February 18, 2019, from https://en.climate-data.org/africa/somalia/lower-juba/chisimayu-872/

Colson, D., Petropoulos, G. P., & Ferentinos, K. P. (2018). Exploring the Potential of Sentinels-1 & 2 of the Copernicus Mission in Support of Rapid and Cost-effective Wildfire Assessment. *International Journal of Applied Earth Observation and Geoinformation*, *73*, 262–276. https://doi.org/10.1016/J.JAG.2018.06.011

Copernicus. (2017). Open Access Hub. Retrieved August 22, 2018, from https://scihub.copernicus.eu/dhus/#/home

Dons, K., Smith-Hall, C., Meilby, H., & Fensholt, R. (2015). Operationalizing measurement of forest degradation: Identification and quantification of charcoal production in tropical dry forests using very high resolution satellite imagery. *International Journal of Applied Earth Observation and Geoinformation*, *39*, 18–27. https://doi.org/10.1016/J.JAG.2015.02.001

European Space Agency. (2015). *SENTINEL-2 User Handbook*.

European Space Agency. (2018). Sen2Cor | STEP. Retrieved August 28, 2018, from http://step.esa.int/main/third-party-plugins-2/sen2cor/

Eva, H., & Lambin, E. F. (1998). Burnt area mapping in Central Africa using ATSR data. *International Journal of Remote Sensing*, *19*(18), 3473–3497. https://doi.org/10.1080/014311698213768

FAO. (2016). *Global forest products: Facts and figures*.

FAO. (2017). *The charcoal transition: greening the charcoal value chain to mitigate climate change and improve local livelihoods, by J. van Dam*. Rome: Food and Agriculture Organization of the United Nations.

FAO SWALIM. (2018). Somalia Water and Land Information Management. Retrieved August 14, 2018, from http://www.faoswalim.org/article/charcoal-production-south-central-somalia

Fernández-Manso, Ó. (2015). *Spectral Mixture Analysis and Object- based Image Analysis for Forestry Applications*. UNIVERSITY OF LEÓN.

Fernández-Manso, Ó., Quintano, C., Fernández-Manso, A., Fernández-Manso, O., & A., F.-M. (2009). Combining spectral mixture analysis and object-based classification for fire severity mapping. *Invest Agrar: Sist Recur For*, *18*(3), 296–313. https://doi.org/10.5424/fs/2009183-01070

Girard, P. (2002). Developments in charcoal production technology. *Unasylva*, *53*(53), 34–35.

Huang, H., Roy, D. P., Boschetti, L., Zhang, H. K., Yan, L., Kumar, S. S., … Li, J. (2016). Separability analysis of Sentinel-2A Multi-Spectral Instrument (MSI) data for burned area discrimination. *Remote Sensing*, *8*(10). https://doi.org/10.3390/rs8100873

Humber, M. L., Boschetti, L., Giglio, L., & Justice, C. O. (2018). Spatial and temporal intercomparison of four global burned area products. *International Journal of Digital Earth*, 1–25. https://doi.org/10.1080/17538947.2018.1433727

Iiyama, M., Neufeldt, H., Dobie, P., Njenga, M., Ndegwa, G., & Jamnadass, R. (2014). The potential of agroforestry in the provision of sustainable woodfuel in sub-Saharan Africa. *Current Opinion in*

Environmental Sustainability, *6*(1), 138–147. https://doi.org/10.1016/j.cosust.2013.12.003
Kaplan, G., & Avdan, U. (2018). Sentinel-2 Pan Sharpening—Comparative Analysis. *Proceedings*, *2*(7), 345. https://doi.org/10.3390/ecrs-2-05158
Key, C. H., & Benson, N. C. (2006). *LA-1 Landscape Assessment (LA) Sampling and Analysis Methods, REMOTE SENSING MEASURE OF SEVERITY: THE NORMALIZED BURN RATIO*.
Manel, S., Williams, H. C., & Ormerod, S. J. (2002). Evaluating presence-absence models in ecology: the need to account for prevalence. *Journal of Applied Ecology*, *38*(5), 921–931. https://doi.org/10.1046/j.1365-2664.2001.00647.x
Muchiri, P. W. (2007). *Climate of Somalia. Technical Report No W-01, FAO-SWALIM, Nairobi, Kenya*.
OrfeoToolbox. (2016). Orfeo Toolbox is not a black box. Retrieved January 23, 2019, from https://www.orfeo-toolbox.org/
Park, H., Choi, J., Park, N., & Choi, S. (2017). Sharpening the VNIR and SWIR bands of Sentinel-2A imagery through modified selected and synthesized band schemes. *Remote Sensing*, *9*(10), 1–20. https://doi.org/10.3390/rs9101080
Rembold, F., Oduori, S. M., Gadain, H., & Toselli, P. (2013). Mapping charcoal driven forest degradation during the main period of al shabaab control in southern somalia. *Energy for Sustainable Development*, *17*(5), 510–514. https://doi.org/10.1016/j.esd.2013.07.001
Robinson, A. P. (1988). Charcoal-making in Somalia: a look at the Bay Method. *Unasylva*, *40*(159), 42–49.
Roteta, E., Bastarrika, A., Padilla, M., Storm, T., & Chuvieco, E. (2019). Development of a Sentinel-2 burned area algorithm: Generation of a small fire database for sub-Saharan Africa. *Remote Sensing of Environment*, *222*, 1–17. https://doi.org/10.1016/J.RSE.2018.12.011
Roy, D. P., Boschetti, L., & Justice, C. O. (2014). The global MODIS burned area product, 182–185.
Roy, D. P., Boschetti, L., Justice, C. O., & Ju, J. (2008). The collection 5 MODIS burned area product — Global evaluation by comparison with the MODIS active fire product. *Remote Sensing of Environment*, *112*(9), 3690–3707. https://doi.org/10.1016/J.RSE.2008.05.013
Roy, D. P., Lewis, P. E., & Justice, C. O. (2002). Burned area mapping using multi-temporal moderate spatial resolution data-a bi-directional reflectance model-based expectation approach. *Remote Sensing of Environment*, *83*(1–2), 263–286. https://doi.org/10.1016/S0034-4257(02)00077-9
Smith, M. O., Adams, J. B., & Sabol, D. E. (1994). Spectral Mixture Analysis - New Strategies for the Analysis of Multispectral Data. In *Imaging Spectrometry — a Tool for Environmental Observations* (pp. 125–143). Dordrecht: Springer Netherlands. https://doi.org/10.1007/978-0-585-33173-7_8
Tane, Z., Roberts, D., Veraverbeke, S., Casas, Á., Ramirez, C., Ustin, S., … Ustin, S. (2018). Evaluating Endmember and Band Selection Techniques for Multiple Endmember Spectral Mixture Analysis using Post-Fire Imaging Spectroscopy. *Remote Sensing*, *10*(3), 389. https://doi.org/10.3390/rs10030389
UN. (2016). *Federal Government of Somalia and United Nations Joint Programme for Sustainable Charcoal Reduction and Alternative Livelihoods (PROSCAL) (Programme Initiation Phase)*.
UN Security Council. (2011). *Report of the Secretary-General on the protection of Somali natural resources and waters*.
UN Security Council. (2012). *Resolution 2036; Imposes a ban on the direct or indirect import of charcoal from Somalia*.
UN Security Council. (2013). *Resolution 2111;Consolidates the arms embargo exemptions from previous resolutions on Somalia and Eritrea*.
UN Security Council. (2014). *Resolution 2182; Renews, until 30 October 2015, the partial lift of the arms embargo on Somalia for the purpose of developing the Security Forces of the Federal Government of Somalia and the humanitarian exemption to the assets freeze*.
UN Security Council. (2015). *Resolution 2244; Renews, until 15 November 2016, the partial lift of the arms embargo on Somalia, the humanitarian exemption to the assets freeze, and the maritime interdiction of charcoal and weapons or military equipment*.
UN Security Council. (2016). *Resolution 2317; Renews, until 15 November 2017, the partial lift of the arms embargo on Somalia, the humanitarian exemption to the assets freeze, and the maritime interdiction of charcoal and weapons or military equipment*.
UN Security Council. (2017). *Resolution 2385; Renews, until 15 November 2018, the partial lift of the arms embargo on Somalia, the humanitarian exemption to the assets freeze, and the maritime interdiction of charcoal and weapons or military equipment*.

APPENDICES

Appendix 1: Temporal trajectories of charcoal sites showing a clear charcoal signal with the NIR band

Appendix 2: Temporal trajectories of charcoal sites showing an unclear charcoal signal with the NIR band

Appendix 3: Six different image dates of the NIR spectral band of Sentinel-2 showing a charcoal signal of a single charcoal site (red polygon) changing locations with the neighbouring pixels